SKB KBS TECHNICAL REPORT 84-19

General Corrosion of Ti in Hot Water and Water Saturated Bentonite Clay

H. Mattsson and I. Olefjord
Chalmers University of Technology

Göteborg, Sweden December 1984

SVENSK KÄRNBRÄNSLEHANTERING AB
Swedish Nuclear Fuel and Waste Management Co
MAILING ADDRESS: SKB, Box 5864 S-102 48 Stockholm, Sweden
Telephone: 08-67 95 40

GENERAL CORROSION OF Ti IN HOT WATER AND WATER SATURATED BENTONITE CLAY

H. Mattsson and I. Olefjord

Chalmers University of Technology
Göteborg, Sweden December 1984

GENERAL CORROSION OF Ti IN HOT WATER AND WATER SATURATED BENTONITE CLAY

H. Mattsson and I. Olefjord, Department of Engineering Metals,
Chalmers University of Technology, S-412 96 Göteborg, Sweden

ABSTRACT

Titanium has been proposed as one of the candidates for canister materials for storing spent nuclear fuel in the Swedish bed-rock. The deposition milieu was simulated on a laboratory scale by embedding titanium in compacted bentonite and the general corrosion rate was investigated. More fundamental studies were also performed where titanium was exposed to water in which special attention was paid to the NaCl content (0 or 1%) and oxygen content (saturated or free from oxygen). In reaction cells designed according to high vacuum principles it was possible to reduce the oxygen content to very low values. The exposure time ranged between 1 min. and 6 months. Analysis of the corrosion products was performed mainly with ESCA.

In water at 95°C the oxide growth follows a direct logarithmic law: $y = 8.7 + 3.65 \ln t$ (y is the oxide thickness (Å) and t is the exposure time (s)). Oxygen and salt do not influence the rate of the oxide growth significantly. The general corrosion rate is approximately the same as the oxide growth rate since the dissolution of Ti into the water-solution is very low. The oxide consists of an outer layer of TiO_2 and a few atomic layers of suboxide close to the oxide/metal interface. Transmission electron microscopy studies of the water-formed oxides indicate that these are amorphous.

The oxides formed on Ti exposed in bentonite is 70 - 100 Å thick for exposure times ranging between 4 months and 2 years. It is shown, that montmorillonite - the main constituent in bentonite - is absorbed in the TiO_2 formed on these samples. If it is assumed that a logarithmic growth law is valid even for long-term exposure in bentonite, the growth law which will give the highest growth rate is $y = 5.5 \ln t$. An oxide thickness of 160 Å is obtained if this law is extrapolated to 100,000 years exposure.

EXECUTIVE SUMMARY

Titanium has been proposed as one of the candidates for canister materials for storing spent nuclear fuel in the Swedish bed-rock. At the deposition site, titanium will be exposed to a sand-bentonite mixture which is saturated with ground water at elevated temperature (80°C). This milieu was simulated on a laboratory scale and the general corrosion rate of Ti was investigated. More fundamental studies were also performed where titanium was exposed to water in which special attention was paid to the NaCl content (0 or 1%) and oxygen content (saturated or free from oxygen). In reaction cells designed according to high vacuum principles it was possible to reduce the oxygen content to very low values. The exposure time ranged between 1 min. and 6 months. Analysis of the corrosion products was performed mainly with ESCA.

It is shown that the oxide growth follows a direct logarithmic law in water at 95°C: $y = 8.7 + 3.65 \ln t$ (y is the oxide thickness (Å) and t is the exposure time (s)). Oxygen and salt do not influence the rate of the oxide growth significantly. The oxide thickness increases with temperature: exposure for 10 days at 25°C and 95°C gives thicknesses of 44 Å and 60 Å respectively. The dissolution of Ti into the aqueous solution is very low; less than one monolayer is dissolved in 3 months even in the most severe environment. Hence, the general corrosion rate is approximately the same as the oxide growth rate. The oxide was found to consist of an outer layer of TiO_2 with a few atomic layers of suboxide - Ti_2O_3 - close to the oxide/metal interface. Transmission electron microscopy studies of the water-formed oxides indicate that these are amorphous.

The measured thickness of the oxides formed on the samples exposed to bentonite saturated with ground water are in the range 70 to 100 Å. The metals were exposed for times ranging from 4 months to 2 years at 95°C. Alloying Ti with 0.2 weight-% Pd does not have any influence on the oxide thickness. The oxides formed in bentonite clay are slightly thicker than the oxides formed in water.The ESCA analysis showed that cations from the bentonite - Si, Al and Mg - are present in the oxide. The atomic ratios between these elements correspond with montmorillonite, which is the main constituent in bentonite. The distribution profile shows a maximum concentration of these elements at the surface and decreasing content towards the oxide/metal interface. Absorption of montmorillonite in TiO_2 may influence the ionic and electronic conductivity of the oxide. The increase in oxide thickness is an indication of this.

If it is assumed that a logarithmic growth law is valid even for long-term exposure in bentonite, the growth law which will give the highest growth rate is $y = 5.5 \ln t$ An oxide thickness of 160 Å is obtained if this law is extrapolated to 100,000 years exposure, which is the desirable length of life for the nuclear waste canister. This is equivalent to dissolution of 90 Å of the metal. Thus, the limitation of Ti as a canister material is not its general corrosion. Instead its resistance against localized corrosion will determine its value. However, it is necessary to determine composition, structure and thickness of the oxide products because the localized corrosion attack will be influenced by the cathodic reaction taking place on the passive film.

Keywords: Titanium, ESCA, XPS, Corrosion, Passive Films, Bentonite Clay.

CONTENTS

	page
1. Introduction	1
2. Experimental	2
2.1. Materials	2
2.2. Exposure equipments	3
2.2.1. Bentonite exposures	3
2.2.2. Exposures in aqueous solutions	4
2.3. Sample preparation	9
3. Calibration studies	11
4. Results and discussion	15
4.1. Bentonite exposures	15
4.2. Exposures in aqueous solutions	23
4.2.1. Oxide growth	23
4.2.2. Oxide composition	29
4.2.3. Oxide morphology	31
4.2.4. Metal dissolution	33
5. Discussion	34
Conclusions	37
Acknowledgements	38
References	39

1. INTRODUCTION

Titanium has been proposed as one of the candidates for canister material for storing spent nuclear fuel at 500 m depth in the Swedish bedrock (1). The metal capsule is thought to serve as an outer corrosion resistant barrier for the canister. The canister will besurrounded by compacted bentonite. Due to the radioactive decay, the temperature may attain a maximum 80°C during the first decades of storing (1). The bentonite clay will be saturated with the species present in the ground water at this depth. Due to the Fe^{2+} present in the granitic rock, the deep ground waters will be oxygen free and reducing conditions will prevail. It is considered unlikely that the NaCl content will exceed 0.5 weight-%, which was the maximum value obtained in an investigation of the ground water chemistry in the Swedish bedrock (2). However, if a new ice-age occurs during the time of storing, higher values may be expected. One property of the bentonite is that it will buffer the pH value around 8-9.

Titanium is of interest as a canister material because Ti and its alloys exhibit excellent corrosion resistance in severe chemical environments. This is due to the fact that Ti is a passivable metal and so the rate of dissolution is governed by the properties of the passive film formed on its surface. To maintain this passive state it is necessary that the metal is exposed to an oxidizing environment. For passivable alloys as stainless steel, oxygenated water provides the oxide forming elements. Due to the very low oxygen content at the deposition site, objections can be raised against Ti as a canister material. For Ti, however, water itself is an oxidizing agent. That this really is the case can be understood from the fact that the equilibrium potentials of the reactions $Ti = Ti^{2+} + 2e^-$ and $2H_2O + 2e^- = H_2 + 2OH^-$ are -1.81 V vs. SHE and -0.47 V vs. SHE respectively at pH = 8.

There exists a considerable scatter in the literature data concerning the oxide growth and dissolution rate of Ti exposed to aqueous solutions. The values of the oxide thicknesses formed at room temperature are in the interval 10-100 Å (3,4,5,6). Smyrl and co-workers (7) found a corrosion rate of 900 Å/year for Ti exposed 270 days to natural brine. Other authors found weight increases corresponding to an oxide thickening of 100-400

Å/year for Ti exposed for 600 days in Baltic sea water (8). At temperatures above room temperature, the data concerning the oxide growth, oxide composition and metal dissolution in aqueous and bentonite environments for longer exposure times are very scarce.

The main purpose of this work was to investigate the dissolution rate and the composition of the reaction products formed on the surfaces of pure Ti and a Ti-0.2Pd alloy exposed to aqueous and bentonite clay environments. Special interest was paid to the influence of oxygen and NaCl contents in the aqueous environments. The reaction and dissolution rates were studied quantitatively. In one set of experiments the real deposition milieu was simulated on a laboratory scale by embedding Ti and Ti-0.2Pd samples in compacted bentonite clay saturated with synthetic ground water.

The analysis technique used was ESCA in combination with ion sputtering. This is the most suitable tool for determination of the surface reaction products and their thickness.

This report is a summary of the experimental work performed so far. A more detailed and conclusive version will be given in a doctoral thesis (9).

2. EXPERIMENTAL

2.1. Materials

The metals used were commercially pure Ti (Avesta ATi24) and Ti-0.2Pd (Avesta ATi24Pd). Chemical analyses of the two materials are given in Table 1.

Table 1. Chemical analyses of ATi24 and ATi24Pd.

Material	weight-% C	O	Fe	N	Pd	Ti
ATi24	0.008	0.06	0.04	0.008	-	bal.
ATi24Pd	0.008	0.06	0.04	0.008	0.18	bal.

2.2. Exposure equipments

2.2.1. Bentonite exposures

The real deposition milieu was simulated on the laboratory scale by embedding the samples in blocks of water-saturated dense bentonite. To achieve long term exposure while maintaining high pressure and high temperature the samples had to be located in thermostated pressure cells. For this purpose eight cells and one insulated vessel were made. The box marked A in fig. 1A is a double-walled thermostated bath in which the pressure cells are located.

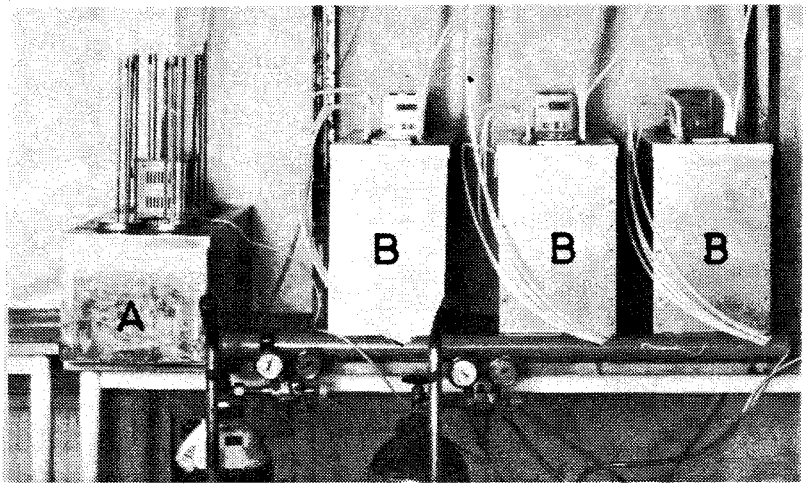

A.

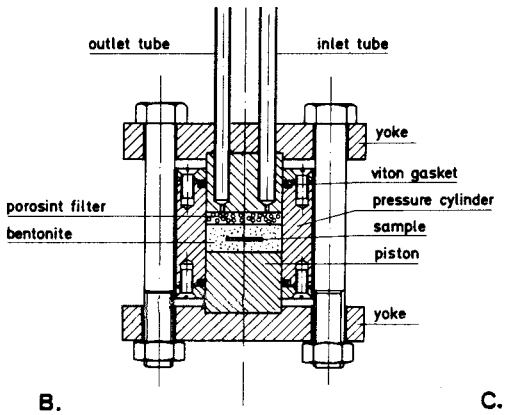

B.

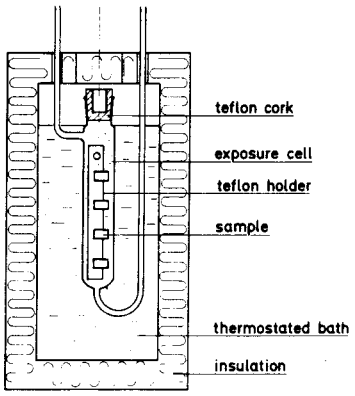

C.

Fig. 1. A: Overview of the experimental set up. B: Pressure cell for the bentonite exposure. C: Water exposure cell.

Fig. 1B shows details of the pressure cell. It consists of a cylinder in which two pistons are fitted. Two water tubes are welded to one of the pistons. The sample is positioned in a block of bentonite. To prevent a change in the volume of the bentonite block due to swelling, two yokes are fixed to the two pistons by six bolts. Transportation of the bentonite into the water tubes is prevented by a porous filter of stainless steel located on the top of the bentonite clay.

The sample was pretreated by polishing on emery paper down to 600 grit and then positioned in the center of a loosely packed volume of bentonite powder and compressed between two pistons in a hydraulic press giving a density of 2.15 g/cm^3. Then one of the pistons was removed and the cell was assembled. The bentonite was saturated with water having a composition corresponding to the ground water in the actual bedrock (10). Table 2 shows the chemical composition of the water. No attempt was made to reduce the oxygen content. This would have been very difficult since oxygen is trapped in the pores of the bentonite block during the compaction procedure. The oxygen content of the ground water can therefore be assumed to attain the value for water in equilibrium with air (i.e. 1 ppm at 95°C). To study the influence of oxygen, fundamental experiments were performed in aqueous solutions where it was possible to reduce the oxygen content to very low values.

Table 2. Chemical composition of artificial ground water (10).

Species	HCO_3^-	SiO_2	SO_4^{2-}	Cl^-	Ca^{2+}	Mg^{2+}	K^+	Na^+
Composition (ppm)	123	12	9.6	10	18	4.3	3.9	6.5

The exposure of eight samples started in Aug. 1981. Since then the exposures have been broken for six of the samples namely after 6 months, one year and two years. By successive ESCA analyses and ion etchings the composition of the oxide in depths and its thickness were investigated.

2.2.2. Exposures in aqueous solutions

To be able to study the influence of oxygen on the corrosion rate of Ti two kinds of exposure cells were designed and built. The intention was to reduce the content of dissolved oxygen in the water to such a low level

that it does not participate in the oxidation of Ti to any appreciable extent. Beside oxygen, the influence of NaCl, temperature and exposure time were investigated. In table 3 the experimental conditions for these exposures are given.

Table 3. Ti exposed to aqueous solutions: experimental conditions.

Parameter	Values
NaCl content (weight-%)	0 1
O_2 content (ppm)	5-20 10^{-4}
Temperatures (^oC)	60 80* 95
Exposure times	1 min** 1 h** 1 day** 10 days** 3 months** 6 months*

*) Exposures only performed in the glass cells.

**) Exposures performed in the electropolishing device.

For adequately controlled, long term exposure specially designed exposure cells were built. Fig. 1A shows the exterior of the three baths (marked B) one bath for each temperature. On a bench above the baths, four water reservoirs made of Pyrex glass are placed (not shown in the figure). Each of these contains one of the four different solutions (i.e. 0 or 1 weight-% NaCl; O_2 or N_2 saturated). The oxygen content was varied by bubbling oxygen or nitrogen through the water in the water reservoirs. The oxygen content in the oxygen saturated water is in the range 5-20 ppm at the exposure temperature (depending on temperature and salt content). Saturation of the water with high purity nitrogen (containing 1 ppm oxygen) gives a theoretical value of the oxygen content in the water of about 10^{-4} ppm. Fig. 1C shows a schematic view of the thermostated bath and the cell arrangement. The exposure water enters the cell via a glass tube at the bottom. The flow rate - ca. 0.3 l per day - is low enough to allow the water to achieve the desired temperature. The flow of water through the cell ensures that the content of oxygen and NaCl is constant throughout the experiment.

With the ambition to decrease the oxygen content in the water to the minimum obtainable value, reaction cells were built in which the residual oxygen was brought to react with hydrogen gas on a Pt catalyst. Figs. 2 and 3 show a schematic drawing and a photo of the low oxygen exposure device respectively. The system consists of an exposure cell and a preparation cell. They are placed in thermostated baths and connected to each other via stainless steel tubing. Furthermore, the exposure cell is connected to a gas container and a rotary pump at one end, and an O_2 trap filled with Hg at the other end. The preparation cell is connected to a gas container (Ar) and an O_2 trap filled with water.

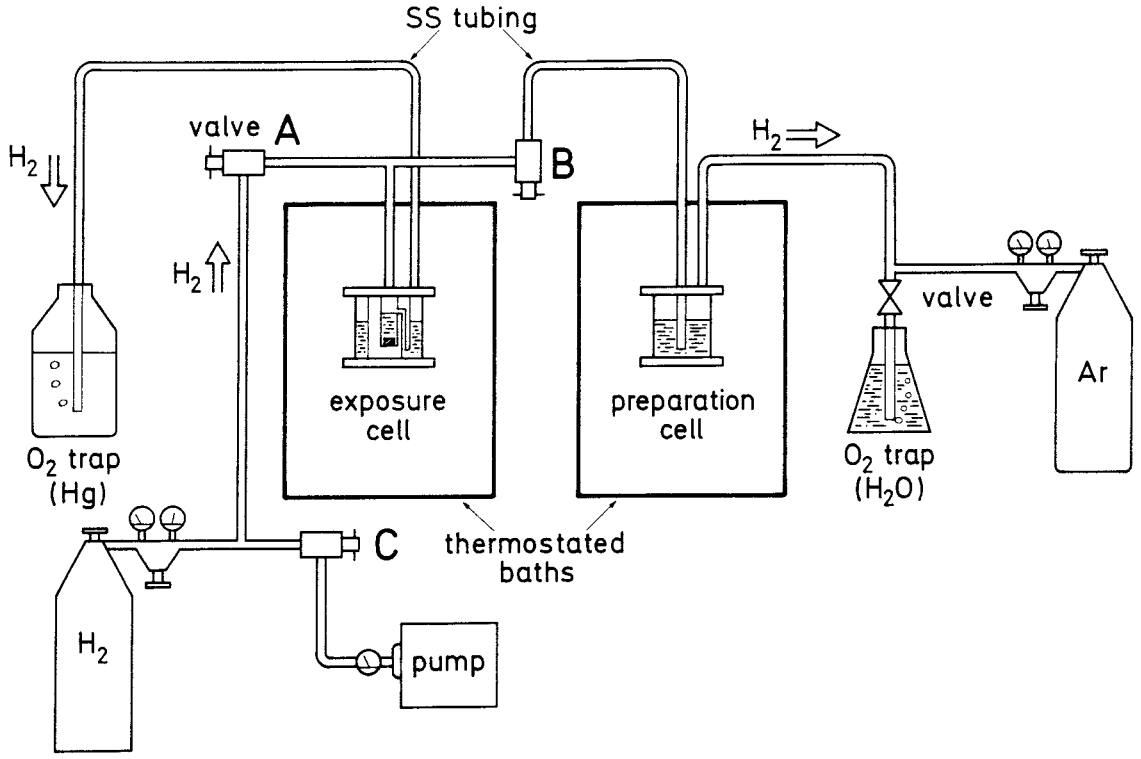

Fig. 2. Schematic representation of the device for exposure to low oxygen containing aqueous solutions.

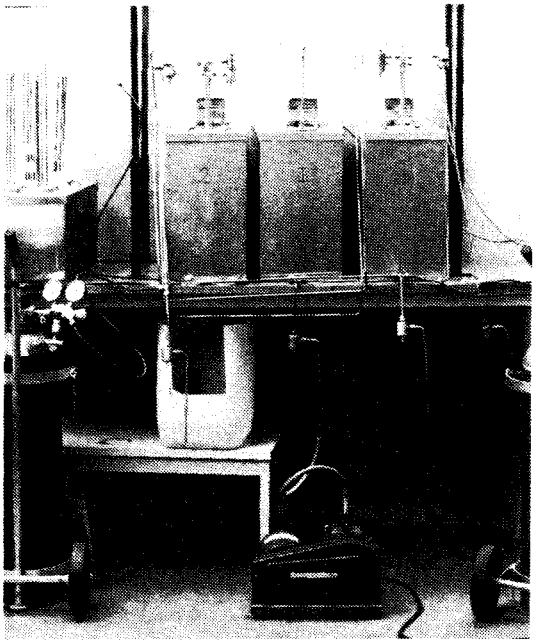

Fig. 3. Photo of the device for exposure to low oxygen containing aqueous solutions.

Details of the exposure cell are shown in fig. 4. It consists of a container and a lid made of stainless steel. The sample to be exposed is placed in an inner cell made of teflon. The container and the lid are pressed together with six bolts. A Pt net is placed 2 mm above the sample. A teflon tube attached to the stainless steel tubing is situated a few mm above the Pt net. During exposure the inner cell and the space between the inner cell and the container are filled with exposure water.

The device was designed according to high vacuum principles. The tube fittings and valves were made of stainless steel. Back diffusion of oxygen from the atmosphere to the exposure cell was prevented by the O_2 trap (Hg) and by the water in the space between the inner teflon cell and the container.

An exposure experiment is initiated by deaeration of the exposure water with H_2. This takes place in the preparation cell by opening the valves A and B (fig. 2) whereby H_2 is allowed to bubble through the water in the preparation cell whereafter it is led out through the O_2 trap (H_2O). The treatment of the water by H_2 bubbling is maintained for one day.

oxygen dissolved in the solution at equilibrium with the gas phase can be calculated from Henry's law:

$$c_{O_2}(aq) = K\, p_{O_2}$$

where $c_{O_2}(aq)$ is the concentration of dissolved oxygen (ppm); K is a constant and p_{O_2} is the partial pressure of oxygen. At 95°C, the minimum attainable oxygen concentration is estimated to 10^{-4} ppm for K = 23.6 (ppm/atm) (12) since the oxygen content of the gas is 5×10^{-6} atm.

2.3. Sample preparation

The samples used in the long term exposures in aqueous environment were pretreated by polishing on both sides on emery paper down to 600 grit. To remove the hard worked zone caused by mechanical polishing and to obtain a smooth surface, the samples used for short term experiments and in the low-oxygen exposure device were electropolished. This was performed on both sides simultaneously in a cell shown in fig. 5. The sample is placed in the center of the electropolishing cell. Each side of the specimen is facing a Pt counter electrode. The electrolyte is pumped through the cell and past the sample from the bottom of the cylinder. The electropolishing of Ti was found to demand a voltage of 25 V yielding a current density of 1.5 A/cm^2 at room temperature. The polishing time used was 25 secs. Under these conditions 25 μm of the sample was dissolved. The electrolyte consists of methanol (500 ml), perchloric acid (50 ml spec. weight 1.54) and butylcellosolve (300 ml). A photo of an electropolished surface is shown in fig. 6. Twin and grain boundaries appear, showing that the hard worked zone obtained during grinding has been removed during electropolishing.

The electropolishing was interrupted by turning the three-way valve to allow exposure water to enter the cell. Hereby the electropolished surface of the sample was immediately exposed to the water and the formation of an air formed oxide was precluded. The samples exposed for 1 min to 1 hour were prepared in this way, while the samples exposed for longer times were transferred to the low oxygen exposure device.

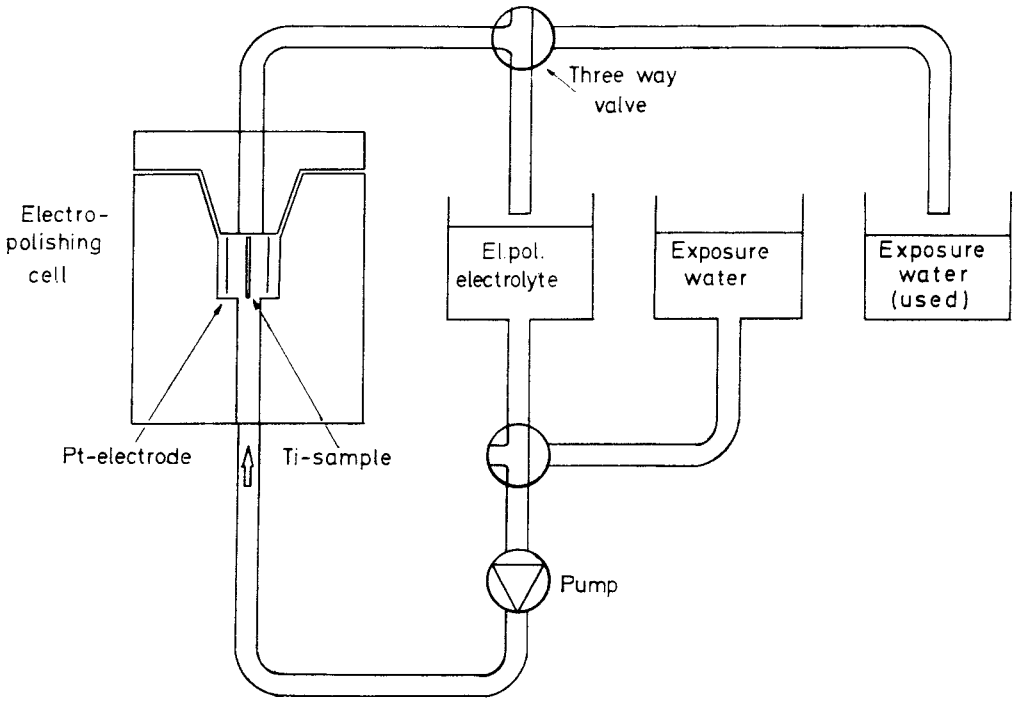

Fig. 5. Electropolishing device.

Fig. 6. Photo of the surface of electropolished Ti. Magnification 150x.

3. CALIBRATION STUDIES

Analysis of the surface reaction products was performed with ESCA in combination with Ar^+ ion sputtering. Calibration of the ESCA binding energies was obtained from the C 1s peak of graphite at 284.3 eV and the Cu $2p_{3/2}$ peak of copper at 932.5 eV. The sputtering rate of TiO_2 at 1 keV Ar^+ ion beam energy was obtained by measuring the time to reach the oxide/metal interface for Ti anodized in the range 4-16 V in 1 M H_2SO_4. The oxide growth dependence on the voltage is approx. 25 Å/V (4,13,14,15). In our case an ion etching rate of 7.5 ± 0.7 Å/min was established for TiO_2. Since the sputtering rate is directly proportional to the ion beam current, this was continuously measured and the sputtering rate was corrected for the variations in the current.

Figure 7. shows ESCA signals of Ti 2p and O 1s recorded after: a-ion etching of Ti; b- oxidizing of Ti in oxygen to TiO_2 (rutile); c- ion etching of TiO_2. The recorded ESCA spectra (solid lines) are deconvoluted into Gaussian-Lorentzian peaks corresponding to elastically scattered photoelectrons from the actual core level (dashed lines) and a background contribution originating from inelastically scattered photoelectrons (also dashed lines). The Ti $2p_{3/2}$ signal representing the metal state is found at a binding energy of 453.4±0.2 eV. The chemical shifts (the difference in binding energy between the actual valence state and the metal state) of the oxide states of Ti are given in table 4.

Table 4. Ti 2p chemical shifts of titanium oxides.

Valence	4+	3+	2+	metal
Chemical shift (eV)	5.5	3.7	1.7	0.0

The position of the O 1s signal of TiO_2 (rutile) is found at 530.3 eV and the relative intensities of the O 1s signal compared with the Ti 2p signal as found in TiO_2 (rutile) is 0.7.

ESCA spectra recorded after 60 Å ion etching of TiO_2 (rutile) are shown in fig. 7c. Apart from Ti^{4+}, lower valence states, Ti^{3+} and Ti^{2+}, appear in the Ti 2p spectrum. The lower valence state oxides are artifacts created during sputtering because X-ray diffraction showed that the oxide consists

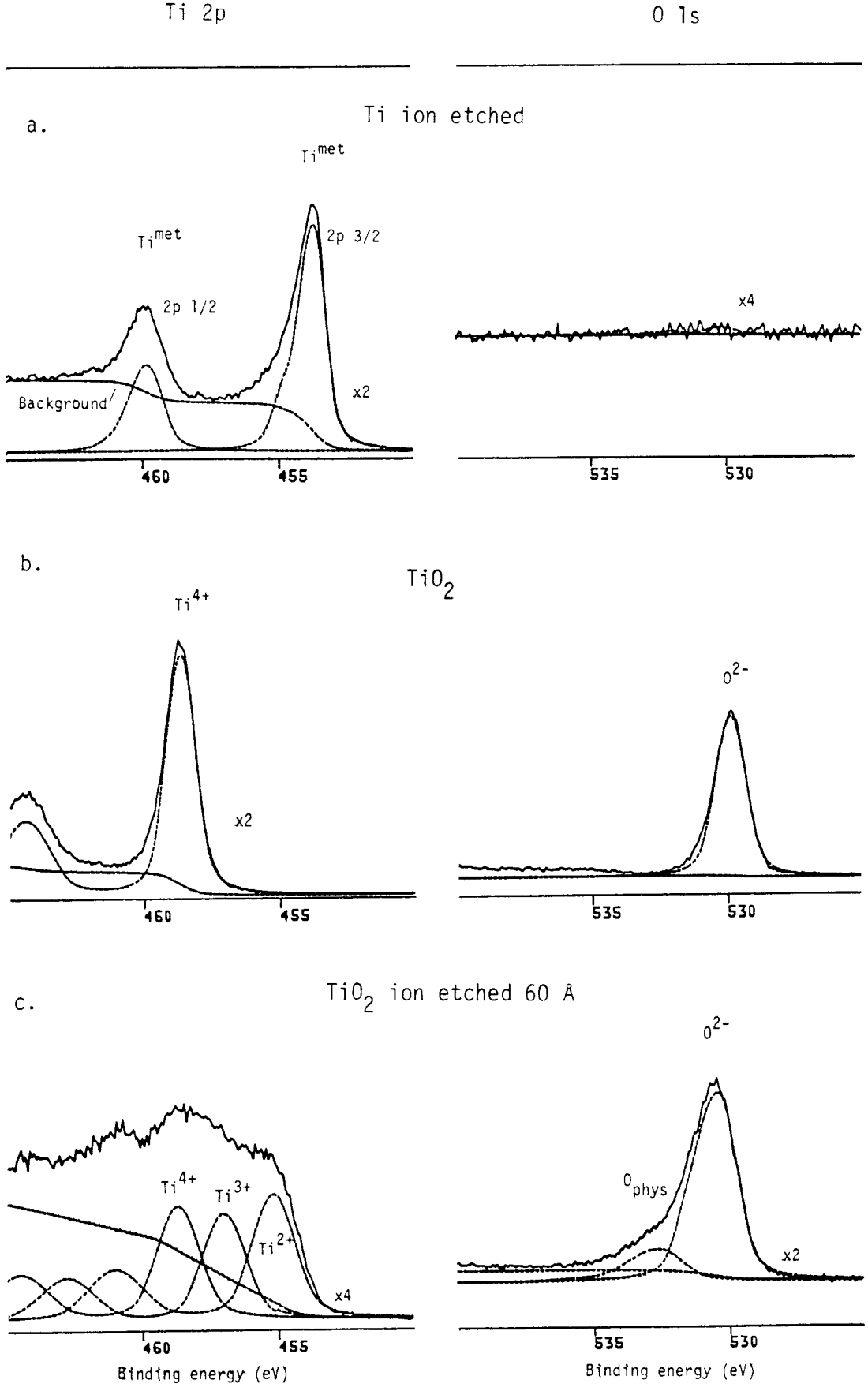

Fig. 7. Ti 2p and O 1s spectra recorded from a) ion etched Ti b) oxidized Ti c) TiO_2 ion etched 60 Å.

of TiO_2 and that its thickness is about 1 μm. Thus, it is impossible to determine the true valence state of a titanium oxide at a certain etch depth directly from the Ti 2p spectrum. Instead comparison with a known oxide ion-etched to the same etch depth under identical conditions must be made. It can also be noted that the Ti 2p and O 1s signals are broadened and that an additional peak appears at the high binding energy side in the O 1s spectrum. After about 60 Å ion sputtering of TiO_2 a steady state is reached where the intensities of the Ti^{4+}, Ti^{3+} and Ti^{2+} signals are approximately the same.

The composition of a compound j is established by calculating the atomic fractions of the elements from the measured intensities. The atomic fraction of an element A is obtained from the formula:

$$x_A = I^j_{Ai}/r_{Ai}/\Sigma(I^j_{kl}/r_{kl}) \qquad (1)$$

where I^j_{kl} is the measured intensity from the core level l of element k in substance j and r_{kl} is the intensity of this core level relative to the intensity of a standard compound. In this study, the intensities were taken as areas under the deconvoluted Gaussian-Lorentzian peaks.

The oxide thickness can be obtained either directly from the ESCA Ti 2p spectrum or by ion etching to the oxide/metal interface. If the oxide is sufficiently thin, contributions both from the metal and oxide states appear in the Ti 2p spectrum. If the oxide is evenly thick, the oxide thickness can be calculated from the formulas

$$I_{ox} = I^{\infty}_{ox} (1 - \exp(-a_{ox}/(\lambda \sin \theta)) \qquad (2)$$

$$I_{sub} = I^{\infty}_{sub} (1 - \exp(-a_{sub}/(\lambda \sin \theta))) \exp(-a_{ox}/(\lambda \sin \theta) \qquad (3)$$

where I_{ox} and I_{sub} are the measured intensities of the ESCA signals from the oxide and the substrate respectively; I^{∞} is the intensity from a semiinfinitely thick layer; θ is the angle between the spectrometer axis and the sample surface; a_{ox} and a_{sub} are the thicknesses of the oxide and substrate respectively and λ is the mean free path of the photoelectrons in the oxide. The mean free path is known only for a few materials and there is a large scatter in the reported values (16). For Ti 2p photoelectrons in the Ti oxide λ was set to 17 Å which is close to the values

employed by other authors (5,6) and to the value obtained by using the theoretical model of Penn (17). The formulas (2) and (3) can practically be used for layer thicknesses up to about 3λ.

Figure 8 shows the intensities of the O 1s and the Ti 2p (metal) signals as function of the etch depth recorded from a sample prepared by electropolishing and then exposed for 10 days in oxygen saturated water at 25°C. The ion etching was performed with 1 keV Ar^+ ions. The first data points were obtained after removal of the contamination layer. The composition profiles are characteristic for results obtained by ion etching of a homogeneously thin film. They never exhibit a step function at the oxide/metal interface due to the topography of the surface, non-uniform ion etching and knock-on effects (18). Further, the level of residual oxygen in the spectrometer chamber makes it difficult to obtain a completely oxygen-free surface. Therefore a small O 1s signal is detected even after 35 min. of ion etching.

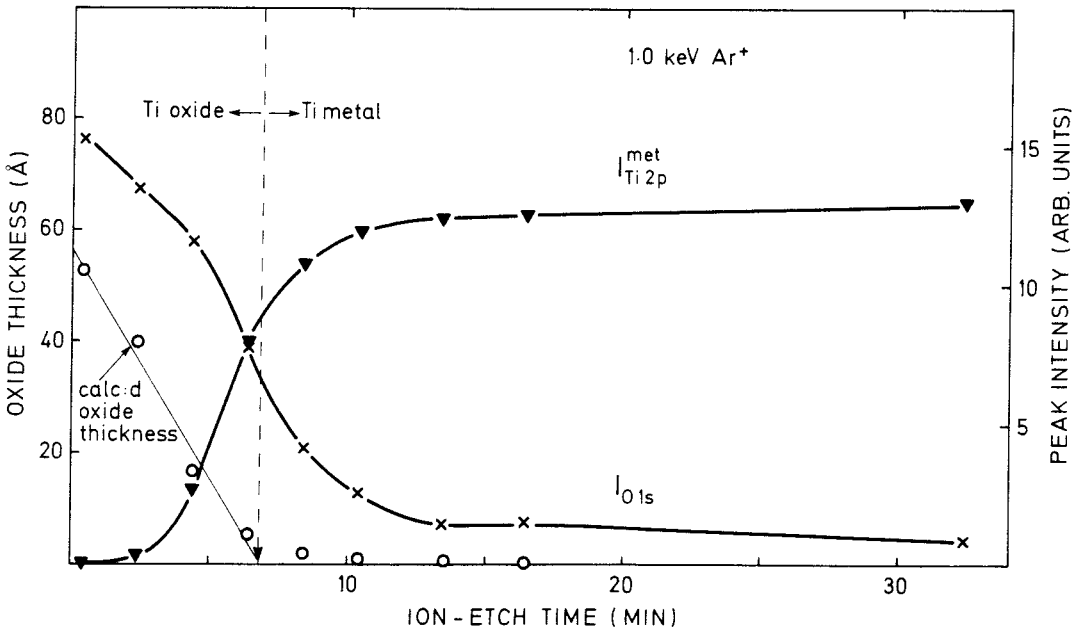

Fig. 8. Depth profile of Ti exposed 10 days to oxygen saturated water at 25°C. Ion etching was performed with 1 keV Ar^+.

The calculated oxide thicknesses, using the eqns. (2) and (3), at each etch depth, are included in the figure. The first four points fall on a straight line. This implies that the oxide is uniformly thick. The slope is equal to an etching rate of 8.3 Å/min., which is close to the value obtained from the independent calibration of anodized titanium. The oxide/metal interface is obtained by extrapolating the straight line to zero thickness.

From the figure it appears that the etch depth corresponding to the thickness of the film is at the position where the intensity of the oxygen and the metal peaks are about 50% of their maximum values. In the following, the oxide thickness was determined by using this 50% intensity.

4. RESULTS AND DISCUSSION

4.1. Bentonite exposure

Commercially pure Ti and Ti-0.2Pd alloys were exposed in compacted bentonite saturated with synthetic ground water at 95°C for 4 months, one year and two years. The elements detected on the surface with ESCA were Ti, O, Si, Al, Mg, Ca, S, C and N. Of these elements carbon and nitrogen are contaminants originating from the atmosphere and from the rinsing procedure. They are easily removed by a slight ion etching. It is suggested that the elements Si, Al, Mg and Ca originate from the bentonite clay since it consists mainly of montmorillonite $Al_{5/3}Mg_{1/3}(OH)_2(Si_2O_5)_2^{1/3-}$ which is a two-dimensional silicate molecule (electroneutrality of the compound is maintained by cations, Ca and Na situated between the silicate layers). Traces of sulphur detected on the surface of some samples presumably originate from the artificial ground water which contained small amounts of sulphate (see tab. 1). In fig. 9 the Ti 2p, O 1s, Si 2s, Al 2p and Mg Auger(KLL) spectra are shown from the original surface and after 50 Å ion etching. The positions of the peaks recorded before ion etching correspond to Ti^{4+}, Si^{4+}, Al^{3+} and Mg^{2+} in their simple oxides respectively. The O 1s signal is split into two peaks. The position of the peak at the lower binding energy (530.2 eV) corresponds to oxygen in TiO_2. The ratio between the measured intensities of the O 1s and Ti 2p peaks is 0.7. This value is the same as the above

reported ratio for synthetic TiO_2. The O 1s peak at 532.1 eV (fig. 9a) is positioned differently from oxygen in the simple oxides. The binding energies of O 1s in these oxides are: 533.5 eV for SiO_2; 532.8 eV for Al_2O_3 and 531.0 eV for MgO. Further, the intensity of the high binding energy component of the O 1s signal matches the intensities of Si^{4+}, Al^{3+} and Mg^{2+} if one assumes that these elements are present as montmorillonite on the surface. In tab. 5 the mean values of the atomic ratios between Al, Mg and Si for all the bentonite exposed samples are given at different etch depths. As can be seen from this table, before and after a slight ion etching the atomic ratios between Al, Mg and Si correspond well with montmorillonite.

It appears from figure 9b that after 50 Å ion etching, lower valence states are present in the Ti 2p spectrum. These are created by decomposition of the surface oxide during Ar^+-ion etching, as already observed for pure TiO_2. However, by comparing the Ti 2p spectrum obtained after ion etching of the bentonite exposed sample with that recorded from pure TiO_2, (figures 9 and 7c), it appears that the former possesses a higher content of Ti^{2+} than the latter. This indicates that a valence state lower than Ti^{4+} is present in the oxide product formed on the surface during exposure in bentonite. Figure 9b shows that Si, Al, and Mg still are present at 50 Å:s etch depth. From the fig. and table 5 it appears that the intensity ratio between the Al and the Si signals has increased compared to the ratio before ion etching. It is suggested that this is due to the preferential sputtering of Si in comparison with Al (19). The intensity of the O 1s peak corresponding to the silicate has decreased substantially at 50 Å etch depth while the peak originating from the titanium oxide has increased considerably.

Table 5. Atomic ratios between Si, Al and Mg at different etch depths for Ti and Ti-0.2Pd exposed to compacted bentonite clay saturated with ground water at 95°C for times between 4 months and 2 years.

Element	Etch depth (Å)					montmor-
	0	2	15	35	50	illonite
Si	1	1	1	1	1	1
Al	.44±.06	.49±.08	.66±.10	.78±.13	.62±.12	.42
Mg	.09±.02	.10±.02	.11±.03	.13±.04	.13±.02	.08

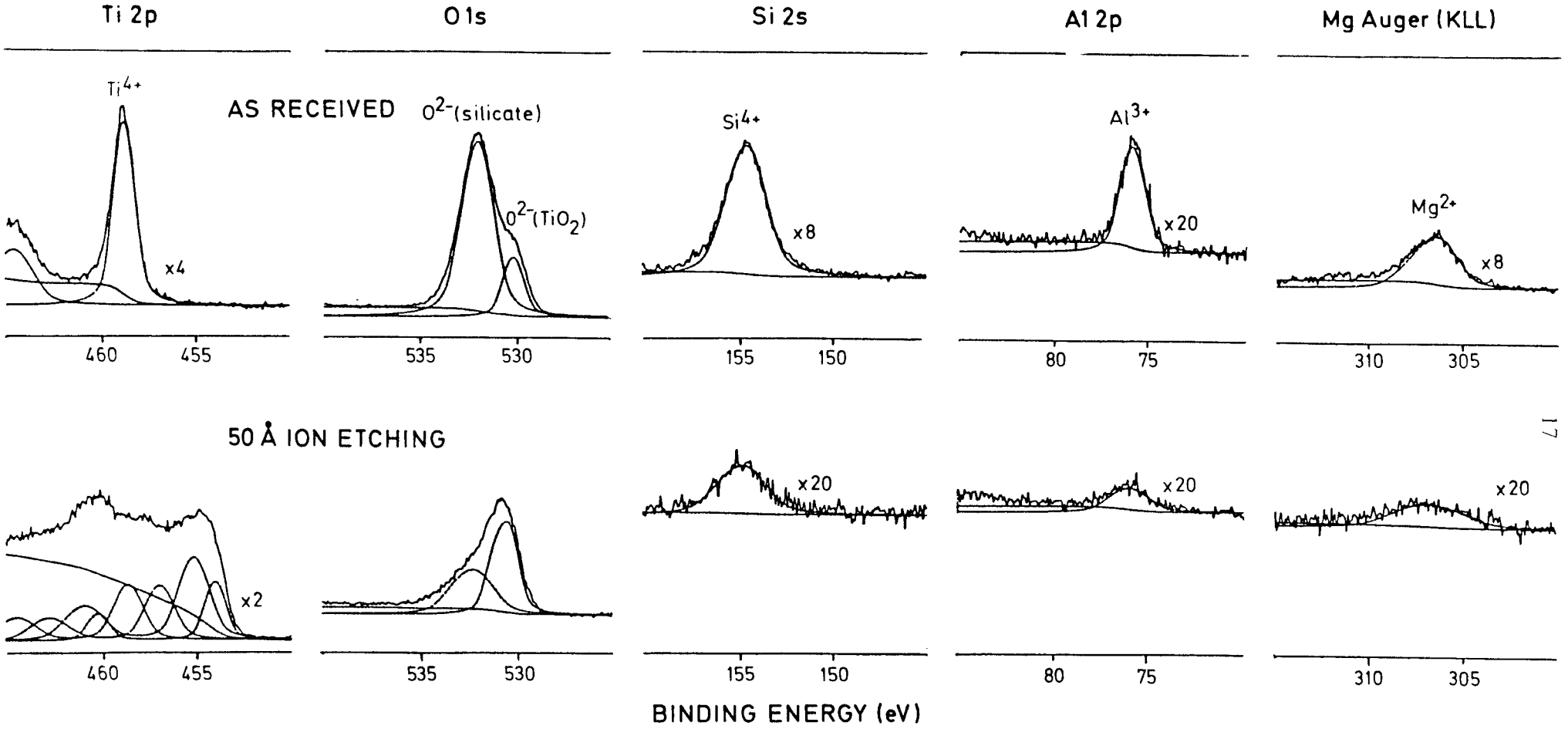

Fig. 9. ESCA spectra recorded from Ti-0.2Pd exposed 2 years to ground water saturated bentonite clay at 95°C. Upper row: spectra recorded as received. Lower row: spectra recorded efter 50 Å ion etching.

Figure 10 shows the concentrations of the cations Si^{4+}, Al^{3+} and Ti^{ox} (the sum of all Ti oxide states) vs. etch depth. The exposure times were 4 months and 2 years. The analysis was performed in the way described in section 3. It appears from the figure that the highest concentration of Si^{4+} and Al^{3+} is at the surface. Their concentrations decreases through the oxide (which is 80-90 Å thick). At the oxide/metal interface Si and Al can still be detected. The concentration of Ti^{ox} is low at the surface but increases to a maximum value of c:a 35 atomic % at 40-50 Å etch depth. Approaching the oxide/metal interface the Ti^{ox} concentration decreases considerably but can still be found in significant amounts after 150 Å ion etching. This is probably an artifact created during ion etching due to the roughness of the surface.

The ESCA spectra are interpreted starting from three models which take the distribution of Si and Al in the oxide into consideration. These models are shown schematically in fig. 11. In model a the bentonite is adsorbed on top of the titanium oxide in a few monolayers thickness. The predicted ESCA intensity depth profiles are shown in the right column of fig. 11. A high intensity from the bentonite elements is expected in the unetched condition which rapidly decreases to zero after a few angstroms ion etching. In model b the bentonite is assumed to be distributed as agglomerates on the surface of the titanium oxide. The agglomerates are arranged as islands and their thicknesses are presumed to range between 300 Å and 600 Å. Thus a constant intensity from the bentonite elements is predicted over several hundreds of Å and a slow decrease in the intensity is expected as the bentonite/oxide interface is reached. The Ti^{ox} intensity profile is more difficult to predict since the Ti^{ox} intensity increases as soon as the covering bentonite is etched away at the same time as it begins to decrease due to removal of the titanium oxide by ion etching. The Ti^{ox} profile of fig. 11b was calculated by assuming that the top layer of the oxide was ion etched as soon as the thinnest agglomerate was etched away. In model c finally, the bentonite is incorporated into the titanium oxide. Here the highest concentrations of bentonite elements are found at the surface of the oxide and decrease to zero over the depth of the oxide. The intensity of Ti^{ox} will be low at the outermost surface but increase to a maximum somewhere between the surface and the oxide/metal interface. Approaching the oxide/metal interface the Ti^{ox} intensity will decrease due to the fact that photoelectrons from the metal now contribute significantly to the ESCA signal.

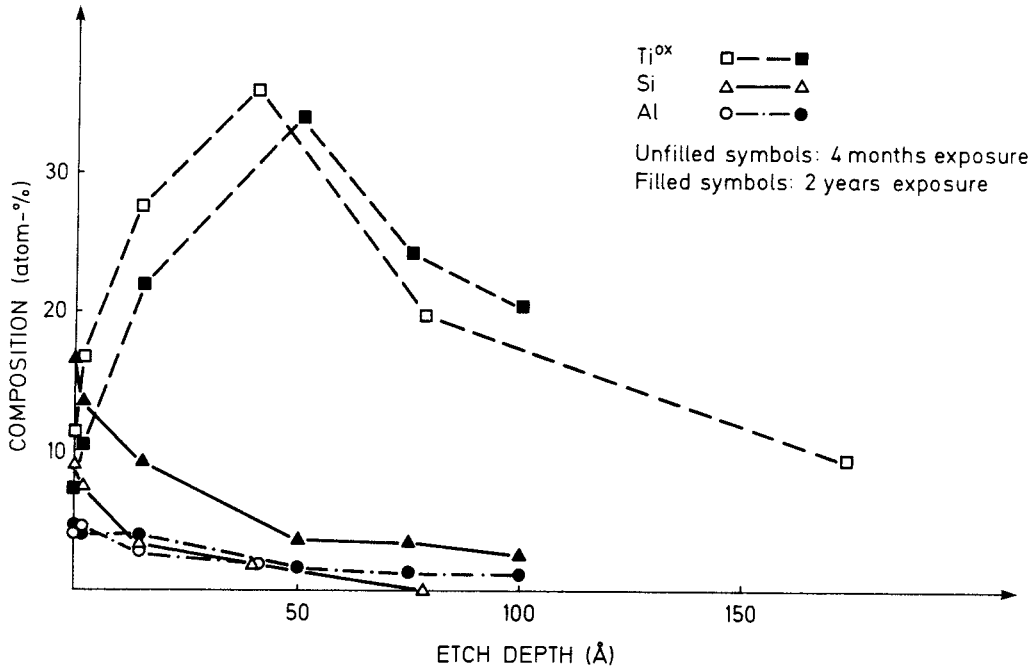

Fig.10. Depth profile of Ti exposed to water saturated bentonite clay at 95°C for 4 months and 2 years.

A comparison between the actual concentration profile and the three models clearly shows that the best agreement is obtained with model c (incorporation of bentonite into the oxide): the concentration of the elements, Si and Al, are monotonously decreasing throughout the oxide and the measured Ti profile shows a maximum in the interior of the oxide. It is stated that the aggregates are enclosed in the oxide as it grows. A suggested model for this is that silicate molecules are adsorbed on the surface of the oxide with a constant rate. In other words, a non-equilibrium state exists on the surface. Because the growth rate of the oxide decreases with time the enrichment of the silicate molecules in the outer layer becomes higher for increasing thickness of the oxide. The model is supported by the concentration profile in fig. 10 and the observation that the concentration of the silicate elements increases with exposure time.

From the spectra of Ti 2p and O 1s recorded before ion etching it was concluded that at least the top layer of the oxide consists of TiO_2 because no contribution from any other valence state than Ti^{4+} was

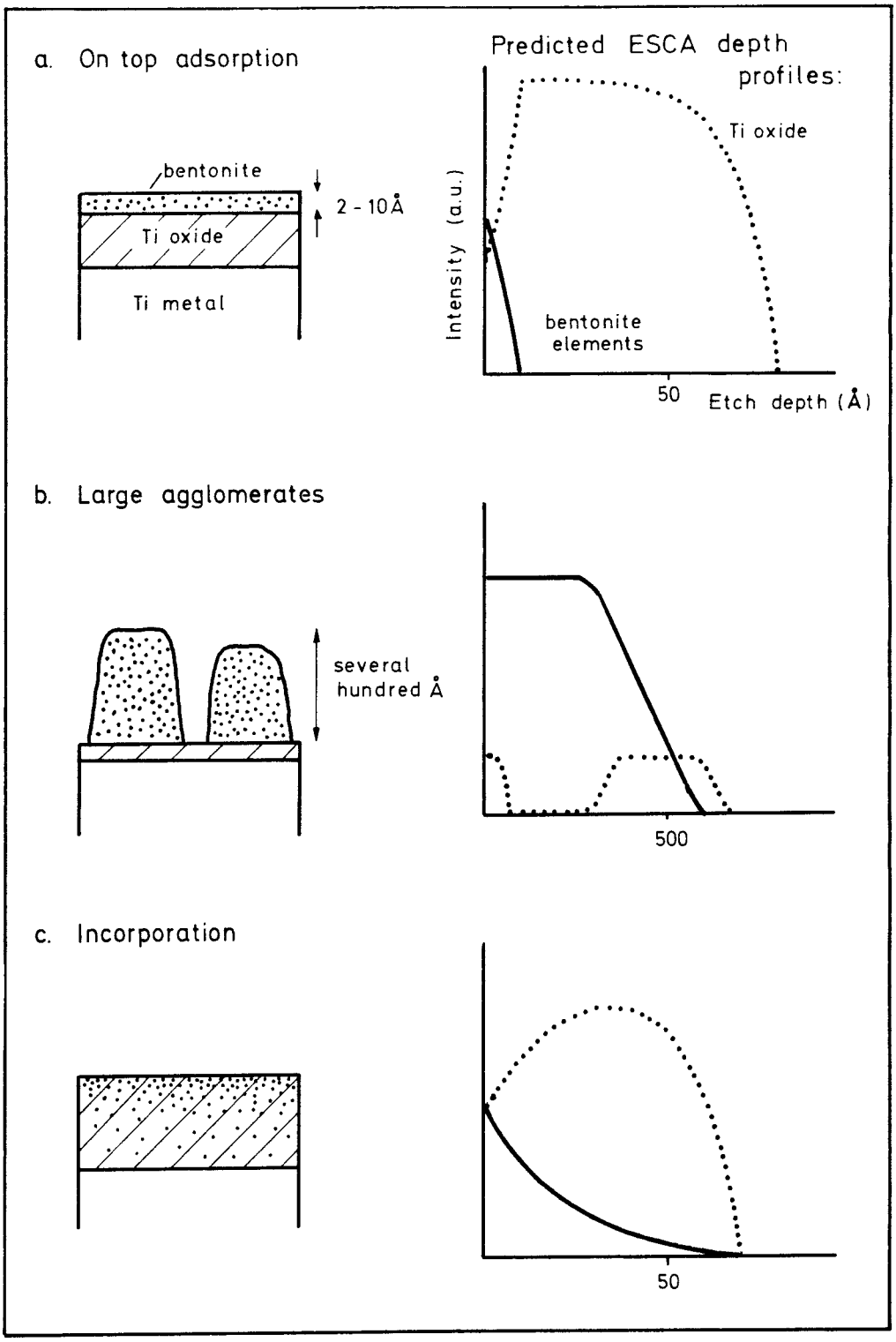

Fig. 11. Showing three proposed models and the corresponding ESCA depth profiles for the interaction between bentonite and Ti.

detected. The minimum thickness of the TiO_2 layer was calculated to be 40 Å thick since the intensity of any prospective suboxide was less than 1% of the intensity from TiO_2. As reported above, ion etching of the sample causes the titanium oxide to decompose. This makes it difficult to establish the true composition of the inner layers of the oxide. To overcome this we have compared the decomposition behaviour of the actual oxide with that of a known oxide. Fig. 12 shows the decomposition behaviour of pure TiO_2. The ratios between the intensities recorded from the different valence states at various etch depths and the intensity of Ti^{4+} before ion etching are given. Fig. 13 shows the corresponding intensity fractions obtained from the alloy Ti-0.2Pd exposed for two years. By comparing the two figures it is evident that the decomposition products of the two oxides are quite similar down to 35 Å. At etch depths greater than 50 Å the results differ: the contribution from Ti^{2+} is markedly greater for the oxide formed in bentonite environment compared to the pure TiO_2. The conclusion is that lower valence oxides exist below this etch depth. In this respect the exposure time does not influence the Ti^{2+}/Ti^{4+} ratio. Thus, it is suggested that a quasi-thermodynamic equilibrium exists at the oxide/metal interface.

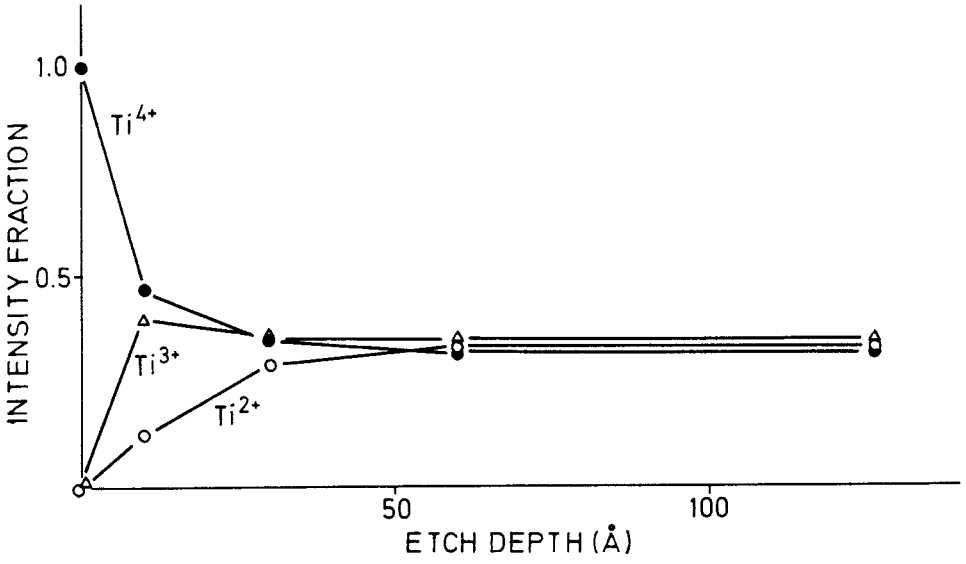

Fig. 12. Decomposition of TiO_2 (rutile) at 1 keV Ar^+ ion etching. Intensity fractions of the three Ti valence states vs. etch depth.

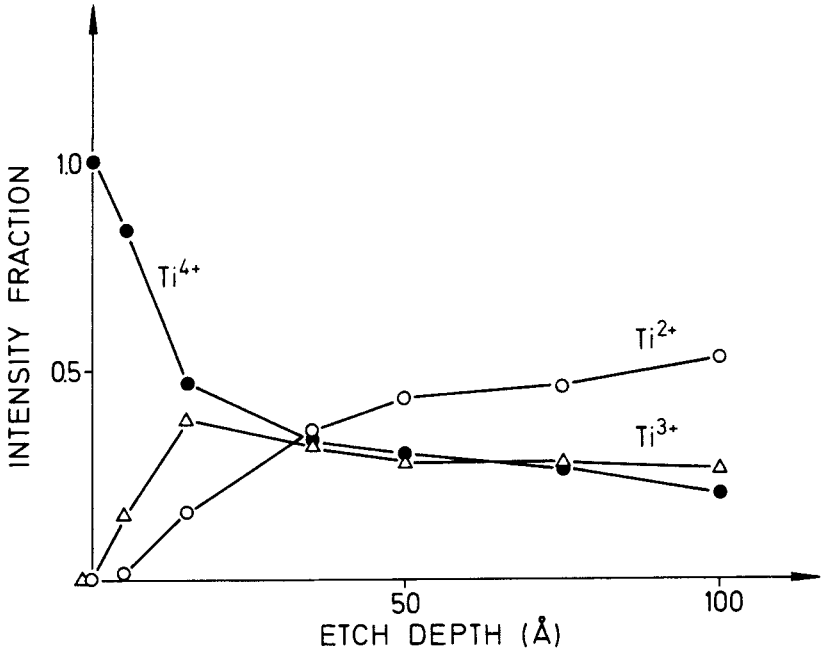

Fig. 13. Intensity fractions of the different Ti valence states (ESCA-Ti 2p signal) vs. etch depth for Ti-0.2Pd exposed 2 years to water-saturated bentonite clay at 95°C.

It was not possible to detect any enrichment of Pd on the surface of the Ti-0.2Pd alloy. Passing the oxide/metal interface, Pd was found in amounts approaching the bulk value. The effect of Pd is to increase the ability of the alloy to repassivate in non-oxidizing, severe acid environments. This is accomplished by an enrichment of the more noble Pd metal in the outermost metal layers by dissolution of Ti metal atoms. In our case the amount of dissolved Ti is limited whereby the enrichment effect of Pd is low. This is confirmed by the fact that no significant difference in oxide composition and thickness exists between the pure and Pd-alloyed material.

The thickness of the oxide products was established by ion etching. It appears from fig. 14 that the oxide thickness is in the range 70-100 Å for exposures between 4 months and 2 years. Only a small tendency of oxide thickening can be seen. The explanation for this observation may be either that the oxide growth has reached a point where the dissolution rate is

equal to the growth rate or that a very slow growth law is prevailing. Such a slow growth rate, namely the direct logarithmic growth law, has been observed for Ti oxidized in oxygen at elevated temperature (149°C) (20) and for Ti exposed to aqueous solutions (this work; see section 4.2.1.). The latter gives an oxide thickness of 68 Å after exposure for 4 months in water and a total increase in thickness of 7 Å during prolonged exposure up to 2 years. These oxide thicknesses are only slightly less than what is found for the bentonite exposed samples. No significant difference can be observed between pure Ti and the Ti-0.2Pd alloy. The oxide thicknesses found in this investigation are in good agreement with those found by other authors. By gravimetric measurements Henriksson and de Pourbaix (8) found corrosion product thicknesses between 100 and 400 Å for Ti exposed 300 days at 100°C to bentonite clay. However, their results were close to the sensitivity of the method.

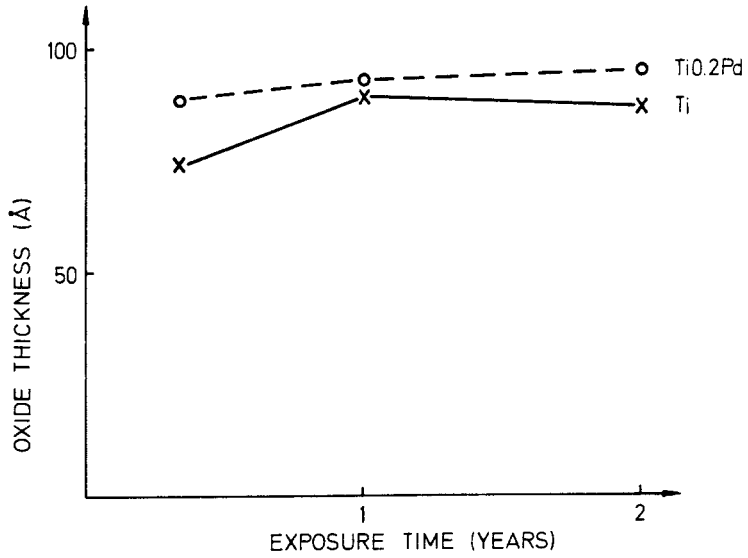

Fig. 14. Oxide thickness vs. exposure time for Ti and Ti-0.2Pd exposed to water saturated bentonite clay at 95°C.

4.2. Exposures in aqueous solutions

4.2.1. Oxide growth

Figure 15 shows the ESCA Ti 2p spectra recorded after exposure of Ti in aqueous solutions for various temperatures and times. The binding energies of the main components of the Ti 2p and the O 1s signals correspond to

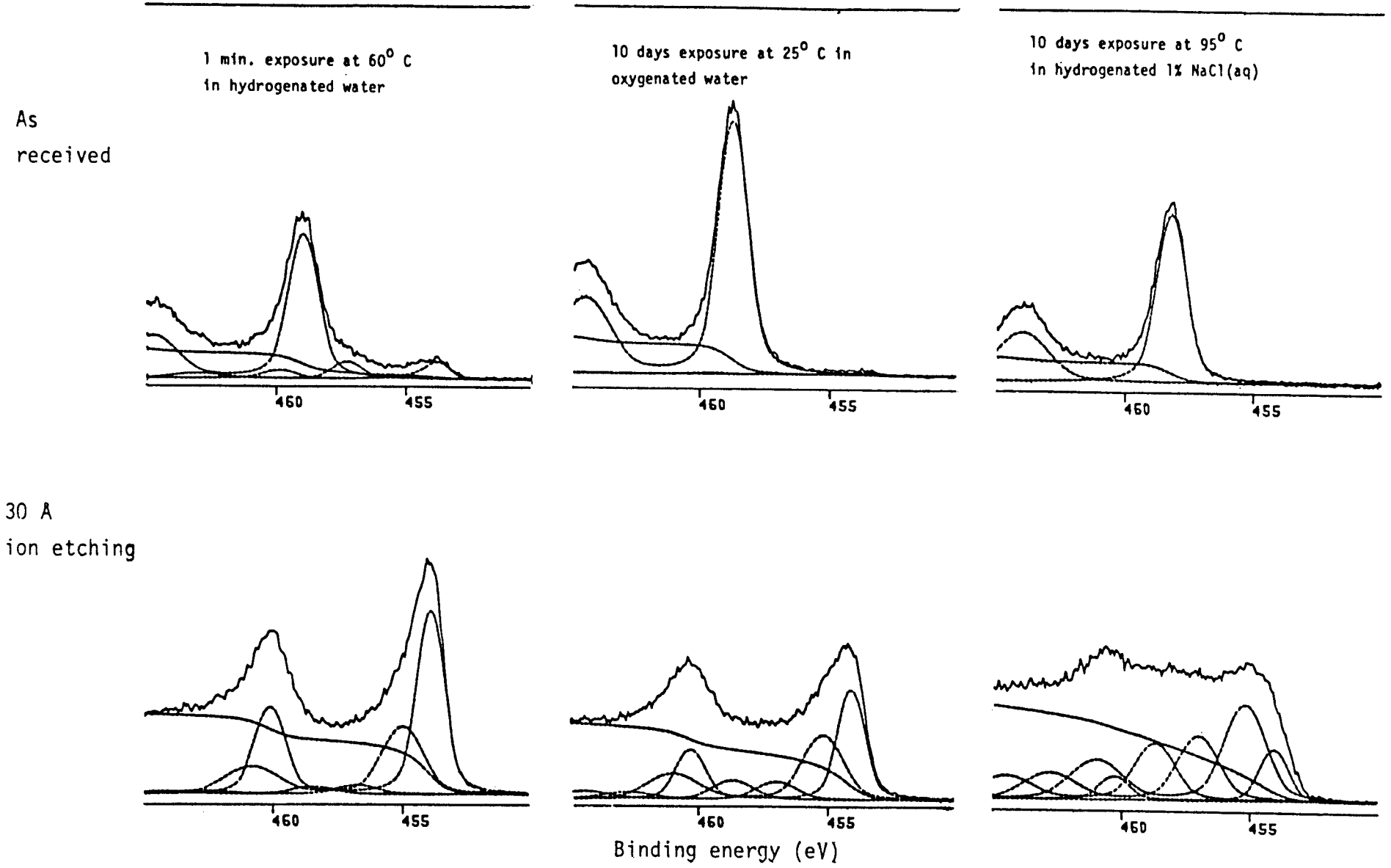

Fig. 15. ESCA Ti 2p spectra recorded from Ti exposed to aqueous solutions at various temperatures and lengths of time. Upper row: as received. Lower row: spectra obtained after 30 Å ion etching.

those found for TiO_2. The Ti 2p spectrum recorded from the sample exposed for 1 min. at 60°C shows that a state occurs between the peaks representing the four valency and the metallic states of Ti. The position of that peak is 457.3 eV which corresponds to the three valency state in table 4. Thus the spectra indicates that a suboxide exists between the outer TiO_2 and the metal phase. Contribution from the metal state appears in the Ti 2p spectrum after exposure for 1 min. at 60°C. No metal contribution can be seen for the samples exposed for 10 days at 25°C and 95°C, thus the oxides are more than c:a 50 Å thick according to eqns. (2) and (3). It appears from the lower row of fig. 15 that the metallic state dominates after ion etching to a depth 30 Å below the original surface of the sample exposed for 1 min. while the Ti 2p spectrum of the sample exposed 10 days at 25°C still contains contributions from the oxide state. The Ti 2p spectrum recorded after ion etching of the sample exposed for 10 days at 95°C is very complex and resembles the spectrum obtained after ion etching of pure TiO_2 to the same depth (see fig. 7c). At this etch depth, the spectrum contains a minor contribution from the metal state.

Due to the fact that the thickness of the oxide formed on the surface during prolonged exposure time is more than 3 times the attenuation length of the photoelectrons the thickness has to be assessed by Ar^+ ion sputtering. The thickness is set as the sputtering depth where the intensity of the Ti 2p metal signal has reached its half maximum value.

The thickness of the oxide formed on pure Ti versus the exposure time is summarized in figures 16 and 17. The temperatures were 95°C and 25°C (fig. 16) and 60°C (fig. 17). The aqueous solutions were either saturated with oxygen or hydrogen. At 95°C and 60°C the water contained either 1% NaCl or was free from salt. The exposure times were 1 min., 1 h, 10 days or 3 months. Most of the analyses were performed after exposure for 10 days at 95°C. It appears from fig. 16 that at this temperature and exposure time the thickness of the oxide product is 60±2 Å. Thus, the measured scatter in thickness is rather small. Further it is not possible to draw conclusions about the influence of the water composition. The thickness of the oxide formed at 60°C is 56±6 Å, which is close to the thickness of the layer formed at 95°C. The oxide formed at 25°C is on the other hand markedly thinnner. After 10 days the measured layer is about 44±5 Å. The results indicate that the film formed in the oxygen saturated solution is somewhat thicker than the oxide formed in the hydrogen saturated solution.

However, only four experiments have been performed and the observed difference is smaller than the scatter in data. To clarify this more experiments have to be done. The thickness of the oxides formed during exposure for short time are estimated from the spectra by eqns. (2) and (3). The layer formed at 25°C directly after electropolishing or grinding of the surface is about 20 Å. At 95°C the measured oxide is about 5 Å thicker. Again no conclusions can be drawn about the influence of the composition of the water.

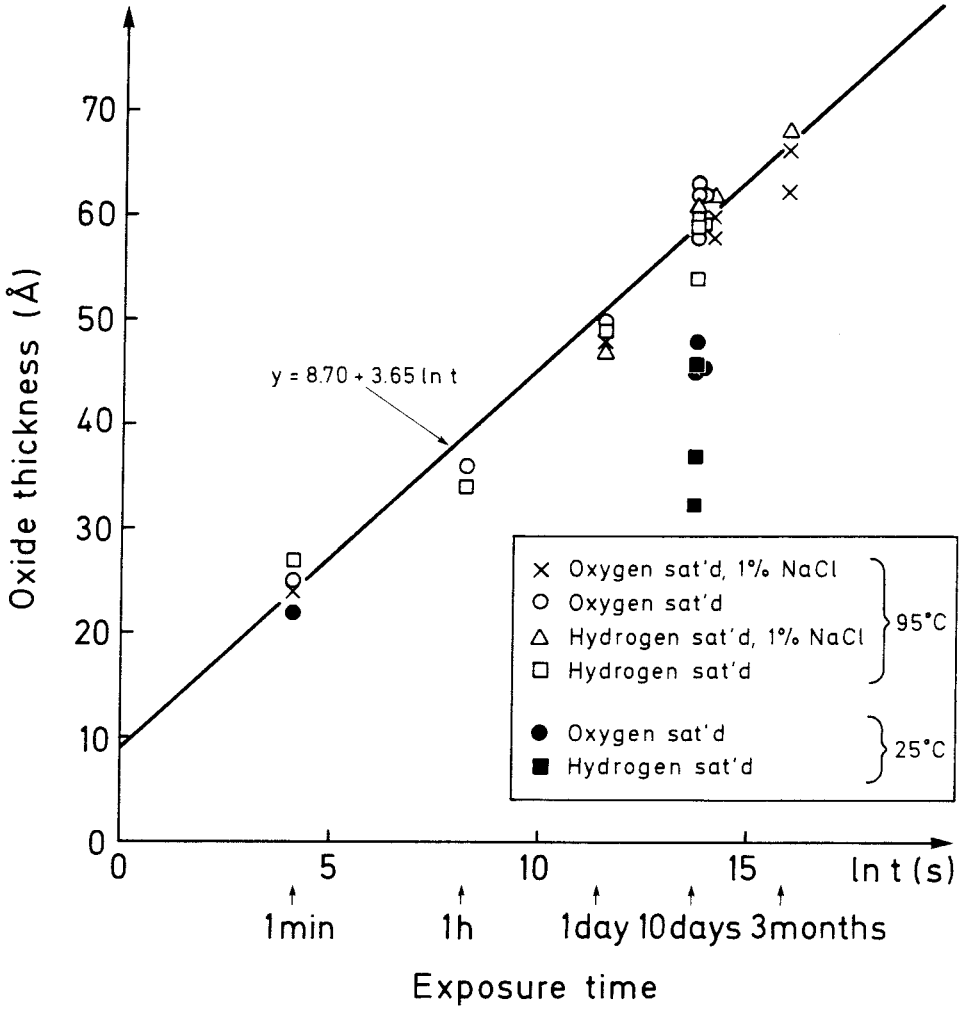

Fig. 16. Oxide thickness vs. exposure time for pure Ti exposed in various aqueous solutions at 25°C and 95°C.

Figure 16 shows that the thickness of the oxides measured as a function of time follows a straight line in a semi-logarithmic diagram. The line corresponds to the expression:

$$y = 8.70 + 3.65 \ln t \qquad (4)$$

where y is the thickness (Å) and t is the time (s). Thus, the oxide growth follows a logarithmic law.

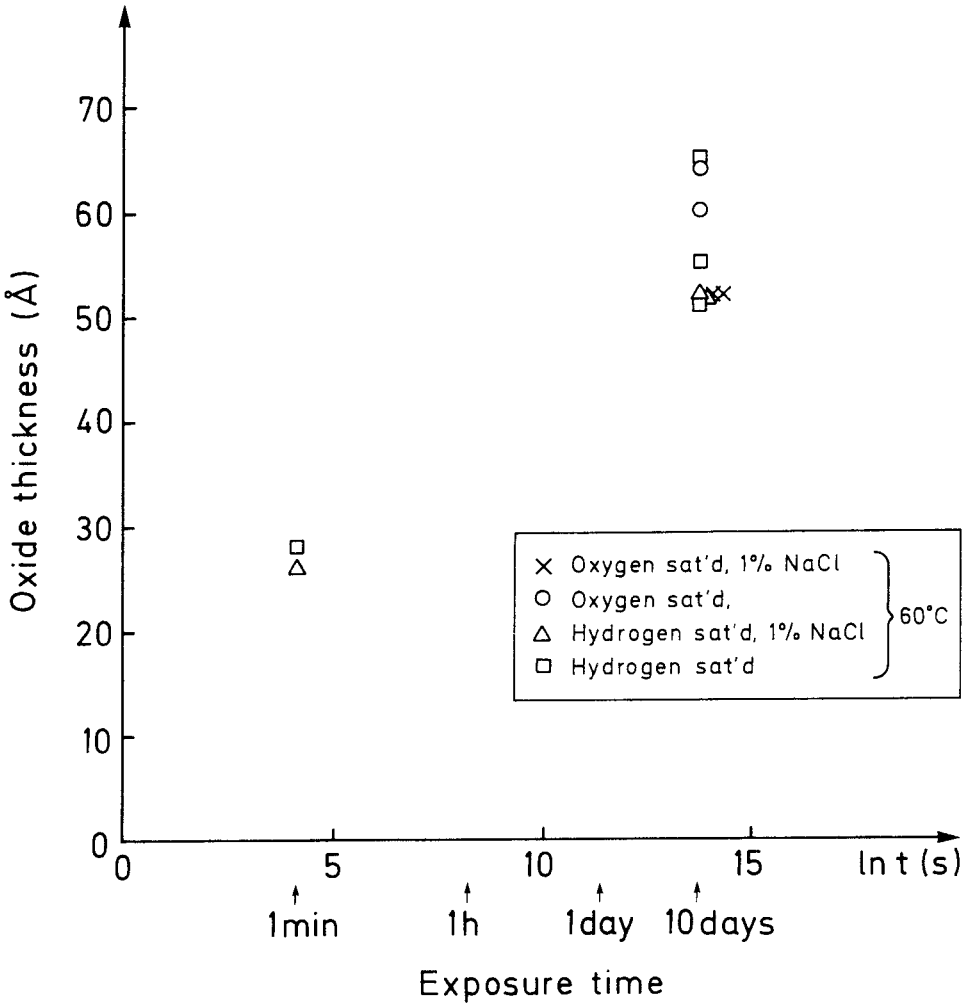

Fig. 17. Oxide thickness vs. exposure time for pure Ti exposed in various aqueous solutions at 60°C.

The results from the series of experiments performed in glass cells are shown in table 6. Titanium and the Ti-0.2Pd alloy were exposed for six months in water saturated with either oxygen or nitrogen. The measured thicknesses of the oxides range from 80 Å to 250 Å. The mean value of all the oxide layers is about 140 Å. The table doesn't show any general trend: the average thickness in chloride containing water does not differ significantly from the average thickness in chloride-free water; the Pd content of the alloy does not influence the oxide thickness significally; the average thickness at 60°C is approximately the same as at 95°C.

Table 6. Oxide thickness (Å) of Ti and Ti-0.2Pd exposed 6 months to aqueous environments in glass cells.

Gas saturation in water	Temp. (°C)	Pure water		1% NaCl	
		Ti	Ti0.2Pd	Ti	Ti0.2Pd
N_2	60	225**	185	142	115
O_2	60	131	134	123	124
N_2	80	145	121	88	86
O_2	80	(201)*	(152)*	81	81
N_2	95	129	133	160	178
O_2	95	- **	125	131	146

Notes: *) These experiments lasted only 3 months due to failure of the glass cell.

**) These samples were heavily contaminated.

From the logarithmic growth law presented in fig. 17 and in eqn. (4) the estimated thickness of the oxide after 6 months exposure is in the range 65 to 80 Å. The values given in table 6 are markedly higher than this. One reason for this is that the glass walls were dissolved during the exposure. This effect was more accentuated in the NaCl-containing solutions. Thus, the elements Si, Sn and Pb were transferred from the glass to the surface of the Ti samples.

Figure 18a shows the distribution of Cl^- ions through the oxide film for two Ti samples exposed in 1% NaCl solutions for 3 months at 95°C which was either oxygen saturated or deaerated. Figure 18b shows the same distribution for two samples exposed for 1 min. at 60°C in oxygen saturated water which either contained 1% NaCl or was salt free. Figure 18a shows that the Cl^- concentration in the oxide is less than 1 atomic-%. The ion etching profile shows that Cl^- ions are present in the oxide. The evidence that Cl^- ions are dissolved in the oxide and not present as salt crystals is the fact that Na^+ ions could not be detected. The Cl^- content of the short time exposed samples (fig. 18b) is higher than in the former case. It is notable that the highest Cl^- concentration is obtained at the oxide/metal interface. It is suggested that the chloride originates from the perchlorate in the electropolishing electrolyte which is deposited on the

metal as soon as the voltage is turned off. In this case it functions as a marker and the maximum concentration found at the oxide/metal interface shows that the oxide is growing outwards. The lower concentration found after 3 months exposure indicates that the Cl^- is dissolved from the oxide into the aqueous solution. This is also the reason why no distinct maximum can be seen.

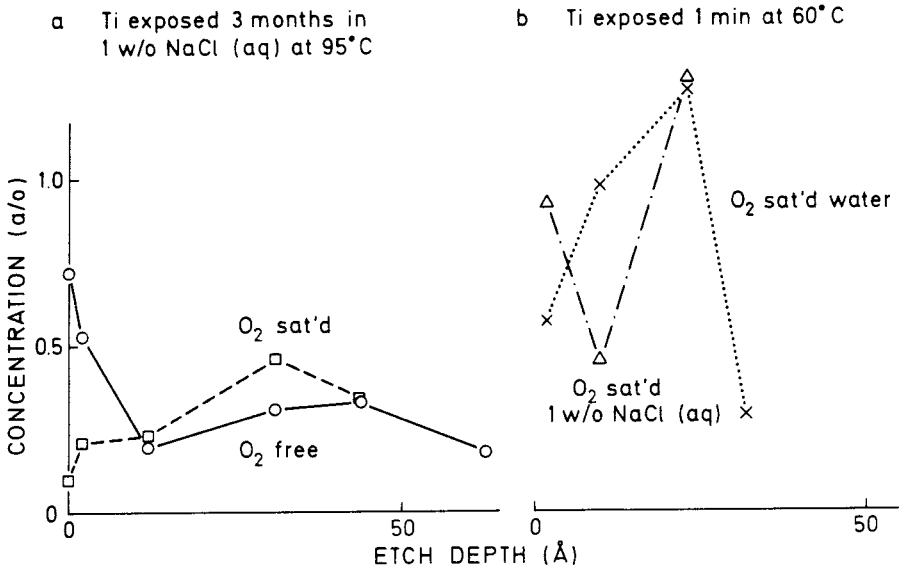

Fig. 18. Chloride concentration in the oxide film as a function of etch depth for Ti exposed to various aqueous solutions.

4.2.2. Oxide composition

Above, it was pointed out that suboxides exist between the outer TiO_2 and the metal substrate. The position of the extra Ti 2p peak corresponds to the position of the three valency Ti. Therefore it is suggested that the suboxide is Ti_2O_3. On a Ti sample exposed 1 min. to hydrogen-saturated water at 60°C the thickness of the Ti_2O_3 layer is estimated as 6 Å and the outer TiO_2 layer as 21 Å using equations (2) and (3). The suboxides are only observed after short exposure at elevated temperature. After prolonged exposure the outer TiO_2 layer has grown to such an extent that contributions from species below the TiO_2 layer become undetectable. Because ion etching changes the chemical state of the species this method

cannot be used to determine the valency states of the oxide film. However, by comparing the ion etch profiles of the water-exposed samples with those obtained by etching pure TiO_2 it is possible to obtain an indication of the existence of suboxides. In figs. 19 and 20 the intensity fractions of the different Ti valence oxides are shown as function of etch depth. The Ti samples were exposed at 95°C either to oxygen-saturated or hydrogen-saturated water. No significant difference between the profiles is observed. Before ion-etching only Ti^{4+} is detected in both cases. Comparison with the ion-etching profile for solid TiO_2 gives good agreement down to 20 Å etch depth. Since the mean free path of the Ti 2p photoelectrons is 17 Å the TiO_2 layer must be at least 40 Å thick. The figures 19 and 20 show that the fraction of the Ti^{2+} intensity near the oxide/metal interface is significantly higher than is found for TiO_2. From this observation one concludes that suboxides are also present in a thick oxide film formed for prolonged exposure in hot water.

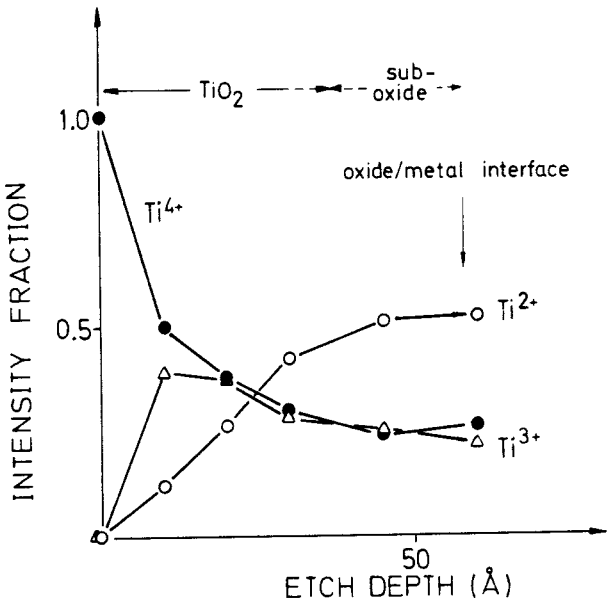

Fig. 19. Intensity fractions of the different Ti valence states vs. etch depth for Ti exposed 10 days at 95°C to hydrogenated water.

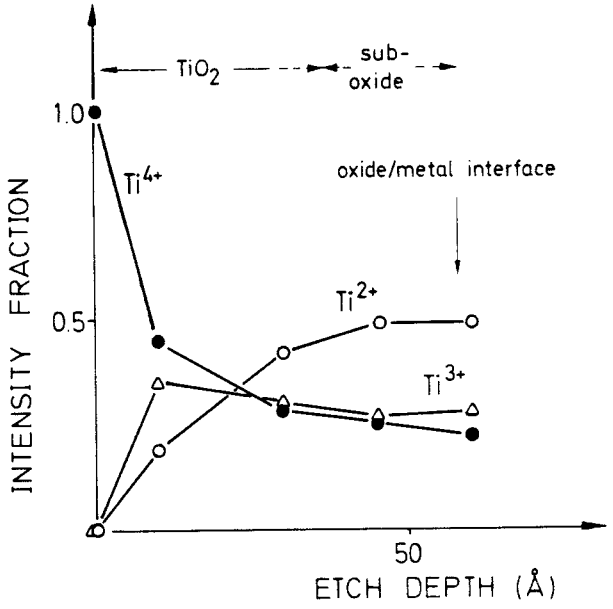

Fig. 20. Intensity fractions of the different Ti valence states vs. etch depth for Ti exposed 10 days at 95°C to oxygenated water.

The composition of the outer oxide layer is very important for the corrosion properties of Ti; hydrated titanium oxide is slightly soluble in acid solutions whereas the annhydrous oxide is not (21). Information about the hydrated/annhydrated state can be sought in the shape of the oxygen signal. However, contamination compounds containing oxygen contribute to

the oxygen signal at positions corresponding to hydroxide and water. In fig. 21 the O 1s and C 1s spectra are shown for a clean TiO_2 oxide and for Ti exposed 10 days at 25°C in oxygenated water. The intensity of the O 1s peak recorded from clean TiO_2 sample (produced in the preparation system of the ESCA) matches completely the intensity of the Ti 2p signal. The C 1s spectrum shows that the sample is practically free from carbon contamination. The O 1s spectrum recorded from the oxide formed in water shows a high intensity peak the binding energy of which corresponds to the oxygen in TiO_2. A shoulder is present on the high binding energy side of this peak. The C 1s spectrum shows that a high level of contaminating carbon is present on the surface. The C 1s spectrum consists of three peaks: the binding energy of the highest peak (285.5 eV) is attributed to hydrocarbons; the peak at 286.8 eV is attributed to hydroxyl bonded carbon and the peak at 288.9 eV is attributed to carbonyl carbon (22). The intensities of the latter two peaks matches the intensity of the high binding energy shoulder in the O 1s spectrum. It is thus concluded that even the outer oxide layers of the oxide formed in water consists of TiO_2. Thus, the the oxide is anhydrous and it is suggested that this property is one reason for Ti:s superior corrosion properties.

4.2.3. Oxide morphology

We have made an attempt to clarify the structure of the surface oxide by electron diffraction studies. Extraction replicas of the oxide formed during exposure for 10 days to hydrogenated water at 95°C were prepared by dissolution of the metal in a 4% bromine-methanol solution. Before dissolution the oxide was reinforced by a deposit layer of carbon. Further, thin foils of Ti were prepared by the usual etching/electropolishing technique for TEM samples. These were then exposed five days at 95°C in either oxygen or hydrogen saturated water.

A diffraction pattern of a thin foil exposed 5 days to oxygenated water at 95°C is shown in fig. 22. The bright spots originate from the metal phase, $(5\bar{1}\bar{4}3)$ reflection in hcp Ti. Two halos can be seen in the figure. The inner halo corresponds to a lattice spacing of 3.09±.10 Å whereas the outer halo corresponds to 1.51±.07 Å. The same halos were observed from the samples exposed to hydrogenated water and also from the extraction replica.

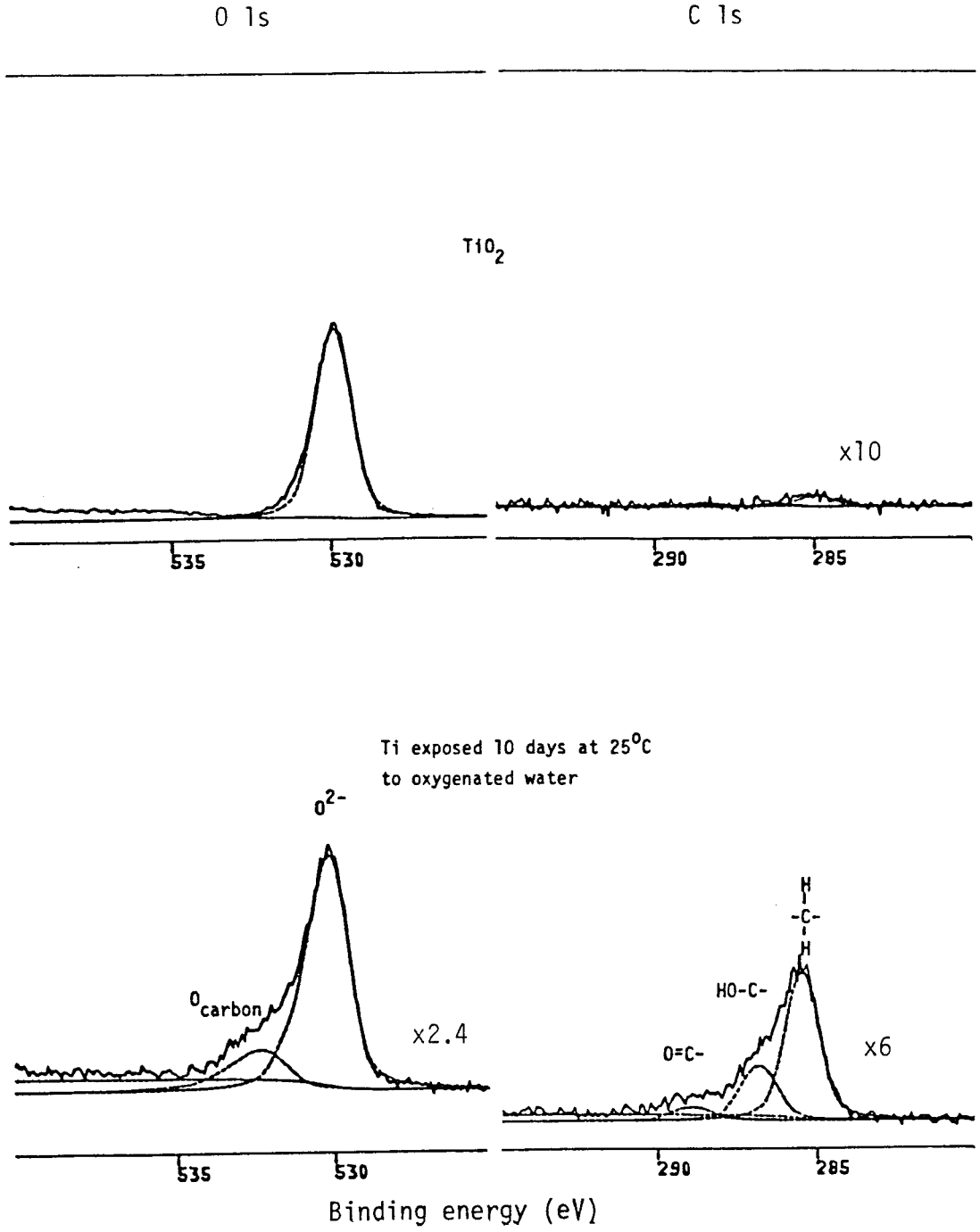

Fig. 21. ESCA O1s and C 1s spectra recorded from a clean TiO_2 oxide and from Ti exposed 10 days at 25°C to oxygenated water.

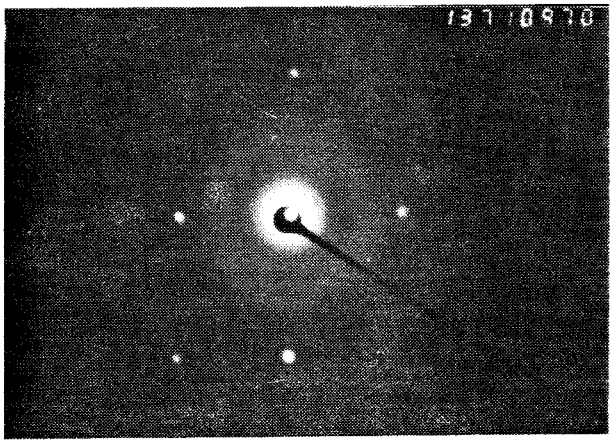

Fig. 22. Electron diffraction pattern of a Ti thin foil exposed 5 days to oxygen-saturated water at 95°C.

The presence of the two diffuse halos in our diffraction patterns shows, that the oxide is either amorphous or consists of crystallites of small lateral dimensions (of the order 20 Å). The absence of spots and high intensity ring patterns expected for the crystalline modifications of TiO_2 shows that the oxide is amorphous.

4.2.4. Metal dissolution

Attempts were made to monitor the dissolution of the metal by measuring the titanium content of the exposure water by analysis with atomic absorption spectroscopy. After exposure the water was poured into a carefully cleaned polyethylene bottle whereafter it was acidified with hydrochloric acid. Analyses were made on water from all exposures ranging from one day to 3 months (i.e. at 60° and 95°C; with and without NaCl; oxygen-free and oxygen-saturated water).

It was not possible in any case to find titanium by atomic absorption analysis of the exposure water. The detection limit of the method is 3 ppb. In our case this corresponds to dissolution of less than one atomic plane of the metal. To ascertain whether or not dissolved Ti is adsorbed on the surfaces of the teflon cell, ESCA analysis was carried out on teflon samples exposed to the aqueous solutions. Only very small traces of

Ti were found corresponding to dissolution of much less than one atomic plane. It was not possible to discover any influence of the environmental conditions.

This analysis shows that almost all of the oxidized Ti atoms are bonded in the solid oxide on the surface. Only a very low percentage of the atoms are dissolved into the solution.

5. DISCUSSION

The corrosion rate and the composition of the passive film formed on the surface during exposure of Ti in aqueous solutions were studied with microanalysis techniques such as ESCA, TEM and atomic absorption spectroscopy.

The thickness of the oxides formed on Ti after electropolishing of the surface and after grinding is approximately 20 Å. This is in good agreement with values given in the literature. By ellipsometry Andreeva (3) found an oxide thickness of 12-16 Å. Using coulometry Nishimura and Kudo (4) determined oxide thicknesses in the range 14-100 Å at potentials in the passive region. The thicker oxides were obtained at higher potentials. Porte and co-workers (5) analysed by ESCA Ti exposed to oxygen at room temperature and obtained an oxide thickness of 45 Å. In another study they (6) reported an oxide thickness of 12 Å for Ti exposed to oxygen at low pressure.

At 95°C the oxide growth follows a logarithmic law: $y = 8.7 + 3.65 \ln t$, where y is the oxide thickness (Å) and t is the exposure time (s). Oxide growth of thin films at low temperature can be described by two logarithmic growth laws, the direct and the inverse one, and it is often difficult to distinguish between them. In the literature, both growth laws have been used to describe the kinetics: the direct logarithmic growth law has been proposed for the oxidation of Ti in oxygen below 330°C and in aqueous solutions at room temperature (20,23,24); Nishimura and Kudo (4) have performed potentiostatic experiments and stated that oxidation of Ti in 1 M Cl^- solutions follows the inverse logarithmic law.

The results show that the thickness of the oxide is independent of the oxygen content in the water. This shows that the oxidation kinetics of Ti is controlled by H_2O decomposition. This is in agreement with the reported literature data for corrosion of Ti at elevated temperature in seawater (25) where almost the same corrosion rate was found for the oxygen saturated as for the deaerated solution. Further, it was not possible to find any influence of the chloride content on the thickness of the oxide. Chloride ions could not be detected from the oxide (except after electropolishing). It is suggested that this is due to the fact that the samples were exposed in neutral water. At lower pH chloride ions may be incorporated into the oxide.

The measured thickness of the oxide formed on the surface of the samples exposed in bentonite clay is in the range 70 to 100 Å. This is somewhat thicker than would be expected from the formula above. After exposure for two years the difference is about 20 Å. Due to the fact that only one sample is exposed and analysed per set of parameters the determination of the thickness cannot be of the same accuracy as in the case of the water exposed samples. The lack of agreement with the water and bentonite exposures cannot easily be predicted. It may be due to the fact that the surfaces of the samples for the bentonite exposure were ground on emery papers and that the increased thicknesses is an apparent topographic effect. On the other hand it cannot be excluded that the increased growth rate is due to molecules of montmorillonite being adsorbed in the oxide. If we assume that a logarithmic law is valid even for long term exposure the growth law which will give the highest growth rate is $y = 5.5 \ln t$. Using this and extrapolating to 100,000 years exposure, which is the desired lifetime for the canister material, an oxide thickness of about 160 Å is obtained. This is equivalent to dissolution of 90 Å of the metal.

The oxide is found to consist of a top layer of TiO_2 with suboxides of Ti_2O_3. The phase diagram shows the existence of the suboxides Ti_2O, TiO, Ti_2O_3, Ti_3O_5 and the homologous series Ti_nO_{2n-1} (n= 4 - 10) at 600°C (26). Some of these oxides may also exist at room temperature. The oxide with the lowest dissolution pressure is situated at the oxide/metal interface. From the thermodynamical point of view (27) it can be suggested that Ti_2O_3 is formed at the interface. On a sample exposed 1 min. to hydrogen-saturated water at 60°C a 6 Å thick layer of Ti_2O_3 was found beneath a 21 Å thick layer of TiO_2. This is in good agreement with findings in the

literature (5) where ESCA analysis of the oxide formed on Ti exposed to oxygen at low pressure shows the existence of both TiO_2 and suboxides which are estimated to be c:a 18 Å and 5-10 Å thick respectively. We found in our investigation that the ESCA signal of the suboxide is strongly reduced with exposure time while the signal from TiO_2 dominates the spectrum. This is simply explained by a model where TiO_2 thickens on top of the suboxides and thus attenuates the photoelectrons from the layers below.

The oxide formed in aqueous environments at elevated temperature was found to be amorphous. Other investigators have reported amorphous oxides on Ti formed at low anodic potentials (14,28) and in methanol solutions with traces of water (29). The latter authors also stress the significance of sample pretreatment and of removing the cold worked zone since plastic deformation of the surface region promotes the formation of a more ordered oxide film. The Ti 2p and the O 1s peaks recorded from samples with a water-formed oxide were found to be broader than the peaks recorded from rutile. This observation implies that the individual atoms in the two oxides experience different environments. The presence of an amorphous oxide can be expected to have benificial influence on the corrosive properties of a metal in comparison with a crystalline one since the grain boundaries present in the latter are weak spots where preferential attack may set in.

Analysis of the aqueous solution after long term exposure shows that the concentration of titanium ions dissolved in the water is very low. The dissolution corresponds to less than one monolayer for three months exposure. Very low dissolution rates have also been observed by Nishimura and Kudo (4) who found that 1 Å dissolved in the first hour of anodic oxidation of Ti in 1 M NaCl. Hence, the major part of the oxidized Ti atoms remains in the oxide and therefore the general corrosion rate is approximately the same as the oxide growth rate.

From above it appears that the general corrosion attack of the metal is negligible. Instead it is the localized corrosion properties of Ti or the Ti-alloys which will determine the use of this metal as canister material from the corrosion point of view. However, it is necessary to characterize the chemical and physical properties of the oxide formed on Ti if the

localized corrosion properties are also to be understood. The crevice and the pitting corrosion attacks will to some extent be controlled by the cathodic reaction occuring on the free passivated surface.

CONCLUSIONS

Bentonite exposure:

- The thicknesses of the oxide formed on Ti and the Ti-0.2Pd alloy are in the range 70-100 Å for exposure times between 4 months and 2 years.

- Assuming that a logarithmic growth law is valid for long-term exposure in water-saturated bentonite, the expression giving the highest growth rate is $y = 5.5 \ln t$; where y is the thickness (Å) and t is the time (s). For 100,000 years exposure, which is the desired life of the nuclear waste canister, the oxide formed is 160 Å thick. This is equivalent to dissolution of 90 Å of the metal.

- The oxide consists mainly of TiO_2 and suboxides at the oxide/metal interface.

- It is shown that montmorillonite, the main constituent of bentonite, is enclosed in the oxide. This species is enriched in the outer part of the oxide. It is suggested that the incorporation of montmorillonite is dependent on the growth rate of the oxide.

- No difference in the oxide thickness could be found between Ti and the Ti-0.2Pd alloy. Pd is not present in the oxide and not enriched in the metal phase.

Aqueous exposure:

- The oxide grows according to a logarithmic law. At 95°C the growth law is $y = 8.7 + 3.65 \ln t$.

- In neutral water, NaCl does not influence the oxide growth rate. No chloride ions were detected in the oxide.

- The oxide thickness increases with the temperature; exposure for 10 days at 25°C and 95°C gives thicknesses of 44 Å and 60 Å respectively.

- The oxidation kinetics are controlled by H_2O decomposition since the thickness of the oxide is independent of the oxygen content. The oxide grows outwards by diffusion of titanium ions.

- The oxide consists mainly of TiO_2 and suboxides (Ti_2O_3) present at the oxide/metal interface.

- TEM studies of oxides formed in aqueous solutions at 95°C show that they are amorphous.

- The dissolution of Ti into the aqueous solutions is very low; less than one monolayer is dissolved in 3 months even in the most severe environment (95°C, 1% NaCl).

ACKNOWLEDGEMENTS

The authors are grateful to the Swedish Nuclear Fuel Supply Company for financial support.

REFERENCES

1. KBS Technical Report 31, Stockholm, 1977.
2. "KBS Annual Report 1980" KBS Technical Report 80-26, Stockholm, 1981.
3. V. V. Andreeva, Corrosion 20 (1964) 35t.
4. R. Nishimura and K. Kudo, Corr. Sci. 22 (1982) 637.
5. L. Porte, M. Demosthenous, G. Hollinger, Y. Jugnet, P. Pertosa, Tran Minh Duc, Proc. 7th Intern. Vac. Congr. & 3rd Intern. Conf.Solid Surf. (Vienna 1977) p. 923.
6. L. Porte, M. Demosthenous and Tranb Minh Duc, J. Less-Common Met. 56 (1977) 183.
7. W. H. Smyrl, L. L. Stephenson and I. W. Braithwaite, Paper No. 85 presented at the annual NACE Meeting, San Francisco, CA, March 1977.
8. S. Henrikson and M. de Pourbaix, KBS Technical Report 79-14, Stockholm, 1979.
9. H. Mattsson, doctoral thesis, to be published.
10. B. Allard and G. W. Beall, J. Environ. Sci. Health A14 (1979) 507.
11. Swedish Standard SIS 02 81 14.
12. P. Hamer, J. Jackson and E.F. Thurson, "Industrial Water Treatment Practice", Butterworths and ICI Ltd, London, 1961, p. 409.
13. N. R. Armstrong and R. K. Quinn, Surf. Sci. 67 (1977) 451.
14. L. Arsov, M. Froelicher, M. Froment and A. Hugot-Le Goff, J. Chim. Phys. 72 (1975) 275.
15. R. Olier, P. Clechet, C. Martelet and J. R. Martin, J. Less-Common Met. 69 (1980) 73.
16. C. J. Powell, Surf. Sci. 44 (1974) 29.
17. D. R. Penn, J. El. Spec. Rel. Phen. 9 (1976) 29.
18. S. Hofmann, Surf. Interf. Anal. 2 (1980) 148.
19. R. Kelly and N. Q. Lam, Rad. Eff. 19 (1973) 39.
20. T. Smith, Surf. Sci. 38 (1973) 292.
21. M. Pourbaix, "Atlas of Electrochemical Equilibria in Aqueous Solutions" Pergamon Press, Oxford 1966, p. 213.
22. K. Siegbahn, C. Nordling, G. Johansson, J. Hedman, P. F. Heden, K. Hamrin, U. Gelius, T. Bergmark, L. O. Werme, R. Manne and Y. Baer, "ESCA Applied to Free Molecules" North-Holland, Amsterdam, 1969, p. 118.
23. I. I. Kornilov, M. N. Zabrodskaya, N. G. Boriskina and A. P. Brynza, Met. Sci. Heat Treatm. 19 (1977) 387.

24. W. A. Alexander and L. M. Pidgeon, Canad. J. Res. (B) 28 (1950) 60.
25. M. A. Molecke, J. A. Ruppen and R. B. Diegle, Sandia Report SAND82-0429, Sandia National Laboratories, N.M., December 1982.
26. "The Oxide Handbook" ed. G. V. Samsonov, IFI/Plenum, New York, 1982, p. 429.
27. "Handbook of Chemistry and Physics", 54th edn., 1973-1974, CRC Press, Cleveland, p. D-50.
28. J. S. L. Leach and D. H. Sidgwick, "Metallic Corrosion" 8th Intern. Congr. Met. Corr., 1981 vol. II (Proc. Conf.), Mainz 1981, p. 82.
29. M. Da Cunha Belo, C. Parant and D. Colin, "Titanium '80 Science and Technology" Proc. 4th Intern. Conf. on Titanium (Kyoto 1980), ed. H. Kimura and O. Izumi, p. 2803.

List of KBS's Technical Reports

1977–78
TR 121
KBS Technical Reports 1 – 120.
Summaries. Stockholm, May 1979.

1979
TR 79–28
The KBS Annual Report 1979.
KBS Technical Reports 79-01 – 79-27.
Summaries. Stockholm, March 1980.

1980
TR 80–26
The KBS Annual Report 1980.
KBS Technical Reports 80-01 – 80-25.
Summaries. Stockholm, March 1981.

1981
TR 81–17
The KBS Annual Report 1981.
KBS Technical Reports 81-01 – 81-16.
Summaries. Stockholm, April 1982.

1982
TR 82–28
The KBS Annual Report 1982.
KBS Technical Reports 82-01 – 82-27.

1983
TR 83–77
The KBS Annual Report 1983.
KBS Technical Reports 83-01–83-76
Summaries. Stockholm, June 1984.

1984
TR 84–01
Radionuclide transport in a single fissure A laboratory study of Am, Np and Tc
Trygve E Eriksen
Royal Institute of Technology
Stockholm, Sweden 1984-01-20

TR 84-02
Radiolysis of concrete
Hilbert Christensen
Studsvik Energiteknik AB,
Nyköping, Sweden
Erling Bjergbakke
Risö National Laboratory,
Roskilde, Denmark 1984-03-16

TR 84-03
Effect of β-radiolysis on the products from α-radiolysis of ground water
Hilbert Christensen
Studsvik Energiteknik AB,
Nyköping, Sweden
Erling Bjergbakke
Risö National Laboratory
Roskilde, Denmark
1984-07-10

TR 84—04
Analysis of some laboratory tracer runs in natural fissures
Luis Moreno
Ivars Neretnieks
The Royal Institute of Technology
Department of Chemical Engineering
Trygve Eriksen
The Royal Institute of Technology
Department of Nuclear Chemistry
Stockholm, Sweden 1984-03-15

TR 84—05
Diffusion in clay—Experimental techniques and theoretical models
Trygve Eriksen
Royal Institute of Technology, Stockholm
Arvid Jacobsson
University of Luleå, Luleå
Sweden 1984-06-28

TR 84—06
Uranium series disequilibrium studies of drillcore Km3 from the Kamlunge test-site, northern Sweden
John AT Smellie
Swedish Geological
Luleå, Sweden 1984-03-30

TR 84—07
Study of strontium and cesium migration in fractured crystalline rock
Erik Gustafsson
Carl-Erik Klockars
Swedish Geological Co
Uppsala, Sweden 1984-09-28

TR 84—08
Fracture fillings in the gabbro massif of Taavinunnanen, northern Sweden
Sven Åke Larson
Geological Survey of Sweden
Eva-Lena Tullborg
Swedish Geological Company
Göteborg August 1984

TR 84—09
Comparative study of geological, hydrological and geophysical borehole investigations
Kurt-Åke Magnusson
Oscar Duran
Swedish Geological Company
Uppsala September 1984

TR 84—10
Geochemical simulation of the evolution of granitic rocks and clay minerals submitted to a temperature increase in the vicinity of a repository for spent nuclear fuel
Bertrand Fritz
Marie Kam
Yves Tardy
Université Louis Pasteur de Strasbourg
Institut de Géologie
Strasbourg, France July 1984

TR 84-11
Smectite alteration
Proceedings of a Workshop Convened at The Shoreham Hotel, Washington, D.C., December 8—9, 1983
Compiled by Duwayne M Anderson
Texas A&M University
November 1984

TR 84-12
Formation of nitric and organic acids by the irradiation of ground water in a spent fuel repository
Hilbert Christensen
Studsvik Energiteknik AB
Nyköping, Sweden 1984-07-13

TR 84-13
The corrosion of zircaloy 2 in anaerobic synthetic cement pore solution
Carolyn Hansson
The Danish Corrosion Centre
Glostrup, Denmark December 1984

TR 84-14
Treatment of zircaloy cladding hulls by isostatic pressing
Ragnar Tegman
Martin Burström
ASEA-CERAMA AB
Robertsfors, Sweden
December 1984

TR 84-15
Sorption of Cs, I and actinides in concrete systems
B Allard
University of Linköping, Linköping
L Eliasson
S Höglund
Chalmers University of Technology, Göteborg
K Andersson
Studsvik Energiteknik AB, Nyköping
Sweden 1984-09-25

TR 84-16
The potential of natural analogues in assessing systems for deep disposal of high-level radioactive waste
Neil A Chapman
Ian G McKinley
John A T Smellie
Stockholm, Sweden August 1984

TR 84-17
The dynamics of Lake, Bog & Bay—Consequences of exposure to man related to final storage of spent nuclear fuel.
P.O. Agnedal
K. Andersson
S. Evans
B. Sundblad
G. Tham
A-B Wilkens
Studsvik Energiteknik AB, December 1984

TR 84-18
Natural Analogues to the Conditions Around a Final Repository for High-Level Radioactive Waste. Proceedings of a Workshop held at Lake Geneva, Wisconsin, USA October 1—3, 1984.
Ed John Smellie,
Swedish Geological AB, December 1984